

AD-A258 917



AFIT/GAE/ENY/92D-11

①

DTIC
ELECTE
JAN 7 1993
S c D

EXPERIMENTAL INVESTIGATION OF THE
AERODYNAMICS OF INDEPENDENTLY ROTATING
CYLINDRICAL SHELLS

THESIS

Walter Clay Howerton
Captain, USAF

AFIT/GAE/ENY/92D-11

612225
93-0004391
93

Approved for public release; distribution unlimited

93 1 04 116

EXPERIMENTAL INVESTIGATION OF THE AERODYNAMICS OF
INDEPENDENTLY ROTATING CYLINDRICAL SHELLS

THESIS

Presented to the Faculty of the School of Engineering
of the Air Force Institute of Technology

Air University

In Partial Fulfillment of the
Requirements for the Degree of
Master of Science in Aeronautical Engineering

DTIC QUALITY INSPECTED 8

Walter Clay Howerton, B.S.
Captain, USAF

December 1992

Accession For	
NTIS GRA&I	<input checked="checked" type="checkbox"/>
DTIC TAB	<input type="checkbox"/>
Unannounced	<input type="checkbox"/>
Justification	
By _____	
Distribution/	
Availability Codes	
Avail and/or	
Dist	Special
A-1	

Approved for public release; distribution unlimited

Acknowledgements

The purpose of this thesis was to experimentally investigate the aerodynamic forces on two adjacent, independently rotating cylinders in a cross-flow. Working on this project, I learned some specifics about such aerodynamics, but I also learned quite a lot about experimentation in general. More importantly, I learned about dealing with adversity and working with other individuals and organizations on whom I depended.

Obviously, anything accomplished in this project was not due only to me. Members of the model fabrication shop, Dave Driscoll and Tim Hancock, produced not only the cylinder models and their mounts, but also the special wind tunnel sidewalls to accomodate them. The lab supervisor, Nick Yardich, met my requests for parts and equipment with only one question: "Is it needed for the thesis?" If my answer was yes, so was his; I could not have hoped for better support. Jay Anderson, the lab's instrumentation specialist, was perhaps the one person most responsible for my having an opportunity to complete this project. His support was worthy not just of acknowledgement, but of true thanks and gratitude.

I also wish to thank my committee members, Dr. Milton Franke, and Lt. Col. Gerald Hasen, and especially my advisor, Dr. Paul King. His insight and encouragement kept me on the right path despite my setbacks and mistakes. Special thanks go to my fiancée, Darlene Haines, who offered personal support and sage advice during the most difficult and hopeless times. It was she who so correctly reminded me, "Faith in God does not exempt us from problems, but it helps us get through them."

Above all, I offer thanks and praise to my Father in Heaven, without Whom I can do nothing.

Walter Clay Howerton

Table of Contents

Acknowledgements	ii
Table of Contents	iii
List of Figures	v
List of Tables	vii
List of Symbols	viii
Abstract	ix
I. Introduction	1
Purpose	1
Motivation	1
II. Theory	3
Potential Flow	3
Beyond Potential Flow	7
Viscous Flow	9
III. Experimental Apparatus	11
Wind Tunnel	11
Models	12
Measurement Devices and Instrumentation	16
IV. Experimental Procedures	19
Flow Visualization	19
Strain Gage Calibrations	19
Force Measurement Validity Check	20
Single Cylinder Tests	20
Dual Cylinder Tests	22
Offset Tests	23

V. Results	24
Flow Visualization	24
Calibrations	25
Primary Configuration	25
Secondary Configuration	26
Check Loads	35
Force Measurement Validity Check	36
Single Cylinder Tests	39
Dual Cylinder Tests	44
Offset Tests	50
Data Confidence and Possible Sources of Error	53
VI. Conclusions and Recommendations	55
Conclusions	55
Recommendations	56
Bibliography	57
Appendix A: Data Acquisition Program	59
Appendix B: Data Reduction Example	68
Appendix C: Experimental Data	70
Vita	80

List of Figures

Figure	page
1. Superposition of Elementary Solutions for Non-Lifting Flow over a Cylinder (Anderson, 1984: 149)	4
2. Superposition of Elementary Solutions for Lifting Flow over a Cylinder (Anderson, 1984: 156)	5
3. Migration of Stagnation Points for Different Values of Circulation: (a) $\Gamma = 0$, (b) $\Gamma < 4\pi V_\infty R$, (c) $\Gamma = 4\pi V_\infty R$, (d) $\Gamma > 4\pi V_\infty R$. (Kuethe and Chow, 1986: 81)	6
4. Shed Vortex Model (Swanson, 1961: 468)	8
5. Aerolab Wind Tunnel Schematic	11
6. Cylinders on Support Shaft	12
7. Primary Configuration of Cylinders in Wind Tunnel	13
8. Secondary Configuration of Cylinders in Wind Tunnel	14
9. Side View of Spokes Assembly, Bearings, and Cylinder	15
10. Cylinder/Drive Interface	16
11. Experimental Setup Schematic	17
12. Cylinder Models in Primary Configuration	24
13. Results of Flow Visualization Test	25
14. Left Vertical Bridge Calibration for Primary Configuration	27
15. Right Vertical Bridge Calibration for Primary Configuration	28
16. Left Horizontal Bridge Calibration for Primary Configuration	29
17. Right Horizontal Bridge Calibration for Primary Configuration	30
18. Left Vertical Bridge Calibration for Secondary Configuration	31

19.	Right Vertical Bridge Calibration for Secondary Configuration	32
20.	Left Horizontal Bridge Calibration for Secondary Configuration	33
21.	Right Horizontal Bridge Calibration for Secondary Configuration	34
22.	Drag Coefficient Versus Reynolds Number	38
23.	Lift Coefficient Versus Velocity Ratio for Same-RPM Tests in Primary Configuration	40
24.	Drag Coefficient Versus Velocity Ratio for Same-RPM Tests in Primary Configuration	41
25.	Comparison of Lift Coefficient Versus Velocity Ratio for Same-RPM Tests in Primary Configuration	42
26.	Comparison of Drag Coefficient Versus Velocity Ratio for Same-RPM Tests in Primary Configuration	43
27.	Lift Coefficient Data for Changing Relative Velocity Ratios	45
28.	Drag Coefficient Data for Changing Relative Velocity Ratios	46
29.	Variations in Lift Coefficient With Changing Relative Velocity Ratio	47
30.	Variations in Drag Coefficient With Changing Relative Velocity Ratio	48
31.	Percent Change in Lift and Drag Coefficients With Changing Relative Velocity Ratio	49
32.	Lift Coefficient Versus Velocity Ratio for Secondary Configuration	51
33.	Drag Coefficient Versus Velocity Ratio for Secondary Configuration	52

List of Tables

Table	page
I. Centered Vertical Check Loads	35
II. Centered Horizontal Check Loads	35
III. Off-Center Vertical Check Loads	35
IV. Calibrations of Primary Configuration	70
V. Calibrations of Secondary Configuration	71
VI. Drag Coefficient Versus Reynold's Number Tests for Primary Configuration	71
VII. Drag Coefficient Versus Reynold's Number Tests for Secondary Configuration	72
VIII. Single-Cylinder Tests Results for Primary Configuration, Filter of 1 kHz	73
IX. Single-Cylinder Tests Results for Primary Configuration, Filter of 10 Hz	74
X. Dual-Cylinder Tests Results for Primary Configuration	75
XI. Thirty Degree Offset Tests Results	79

List of Symbols

Symbol	Description	Units
c	shed vortex radial distance	m
c_d	drag coefficient	
c_l	lift coefficient	
c_p	pressure coefficient	
K_α	shed vortex Kutta-Joukowski coefficient	
p	absolute pressure	N/m ²
R	cylinder radius	m
r, θ	polar coordinates	
T	ambient temperature	K
V_∞	freestream velocity	m/s
v_r	radial velocity component	m/s
v_θ	angular velocity component	m/s
α	velocity ratio	m/s
γ	shed vortex angle	deg
Γ	circulation	m ² /s
κ	doublet strength	m ³ /s
ϕ	velocity potential	m ² /s
μ	coefficient of viscosity	N s/m ²
μ_0	reference coefficient of viscosity	N s/m ²
ρ	density	kg/m ³
ρ_∞	freestream density	kg/m ³
ψ	stream function	m ² /s
ω	vorticity	rad/s
ω_0	cylinder rotational speed	rad/s

Abstract

The purpose of this thesis was to investigate experimentally the aerodynamic forces on two adjacent, independently rotating cylinders in a cross-flow. Previous experiments have addressed single cylinders, but the effects of having two cylindrical sections rotating at different rates have not received much attention.

This investigation involved a force measurement setup which had the two cylinders mounted on a common support shaft, extending beyond the span of the wind tunnel test section, and supported by spoke rings with strain gages in the vertical and horizontal directions. This setup proved capable of measuring aerodynamic forces.

The lift on the independently rotating cylinders was found to increase as one cylinder's angular speed increased while the other's remained constant, and decrease as the relative angular rate decreased. The drag coefficient was fairly constant over the range of velocity ratios tested, and minimal changes were noted with relative changes in angular speeds. Interactions between the two cylinders had the most effect on the lift and drag above 40% disparity in the angular rotation rates.

The investigation also showed that for an offset angle of 30° on an approximately two-dimensional cylinder, the normal component of freestream velocity may be treated as the only significant contributor to the forces on the cylinder.

EXPERIMENTAL INVESTIGATION OF THE AERODYNAMICS OF INDEPENDENTLY ROTATING CYLINDRICAL SHELLS

I. Introduction

Purpose

The purpose of this thesis was to investigate experimentally the aerodynamic forces on adjacent, independently rotating circular cylinders in a cross-flow. The scope of the experiments was limited to include two cylinders on a common support shaft in two distinct configurations. The first configuration was for a direct cross-flow; that is, the cylinders were mounted perpendicular to the freestream. The second configuration had the cylinders offset from perpendicular by 30° , to verify that only the normal component of velocity contributed to the aerodynamic forces of lift and drag in question. The primary control variables for the experiments were the freestream velocity and the angular velocities of the cylinders. Since each cylinder rotated independently, these angular velocities in general did not match. The main results sought from these experiments were the forces on the cylinders, which could be expressed as components of lift and drag.

Motivation

The need for such experiments arose from a lack of data regarding the effects of having adjacent cylinders rotating at differing angular velocities from one another, particularly as applied to missile designs. The specific project which brought this need to light was called the Rocket Electric Field Sounding (REFS) program. A Folding Fin Aircraft Rocket (FFAR), designed to carry a payload for the REFS program, includes a

payload shell which spins at a different angular velocity than does the motor casing. A technical report describing the rocket and its preliminary analysis (Jumper and others, 1991: 11) calculated Magnus forces for each section based on previous experimental results for single cylinders in a cross-flow, but neglected any effect one cylindrical section might have on the other. Experimental data are needed to determine the validity of such simplifying assumptions. These are precisely the kinds of results sought in this thesis.

II. Theory

Before conducting an experiment, it is beneficial to investigate the theory behind the phenomenon in question. Just as there are virtually no theories that can be accepted without some empirical justification, there are also no experimental results that can stand alone without some theoretical explanation and backing. For the case of rotating cylinders, it is instructive to start with the simplest theoretical model, potential flow, and then look at attempts to model the more realistic effects of rotationality and viscosity.

Potential Flow

In any mathematical model of a physical phenomenon, certain assumptions are made. Potential flow intrinsically involves three basic assumptions about the fluid medium, namely that it is incompressible, inviscid, and irrotational. The inviscid flow assumption will cause a significant error in the prediction of drag on the cylinders; in fact, it will cause the model to predict exactly zero drag, which is not physically true. However, the lift information obtained from the potential flow model is a reasonable starting point, and has been used as a reference for many previous experiments dealing with individual rotating cylinders (for example, Reid, 1924; Thom, 1925, 1932, and 1934; Swanson, 1961: 462; White, 1979: 464).

The governing equation for potential flow is Laplace's equation:

$$\nabla^2 \phi = 0 \text{ , or } \nabla^2 \psi = 0 \quad (1)$$

where ϕ is the velocity potential, and ψ is the stream function. Because Laplace's equation is linear, solutions may be superposed with one another to form more solutions. The superposition of these elementary solutions is the basis for modeling certain types of flow situations, including the flow over a rotating cylinder. The most basic of these solutions is for uniform flow, with no body to disturb it. The solution for the stream function for uniform flow is

$$\psi = V_{\infty} r \sin \theta \quad (2)$$

where r and θ are the components of polar coordinates. Other elementary solutions, point sources and sinks, can be combined in a limiting process by which they coexist at a single point called a doublet. The stream function solution for a doublet is

$$\psi = -\frac{\kappa \sin \theta}{2\pi r}. \quad (3)$$

The superposition of uniform flow and a doublet of strength κ results in non-lifting flow over a cylinder, as seen in Figure 1 (Anderson, 1984: 149).

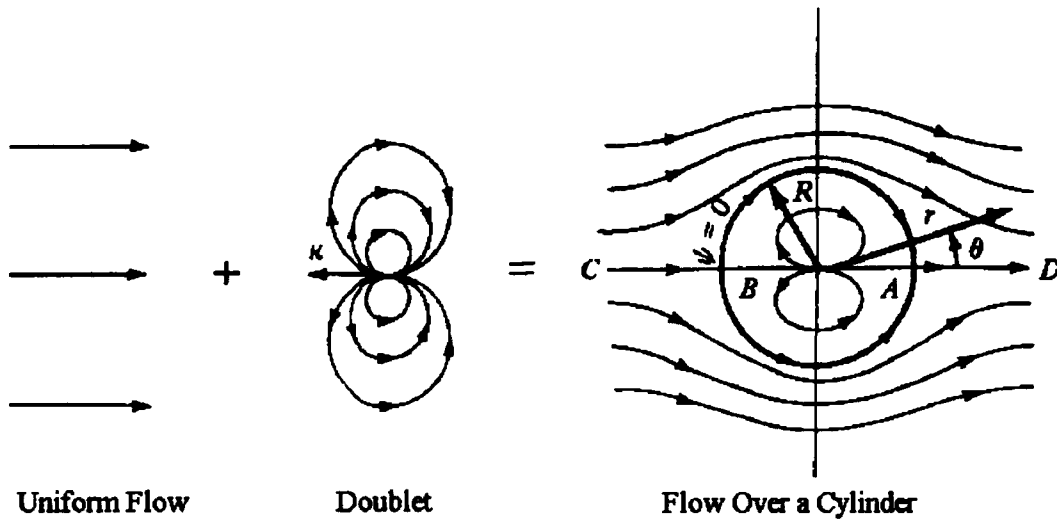


Figure 1. Superposition of Elementary Solutions for Non-lifting Flow over a Cylinder (Anderson, 1984: 149)

The next type of elementary solution of interest is the vortex, for which the solution for stream function is

$$\psi = \frac{\Gamma}{2\pi} \ln r, \quad (4)$$

where Γ is the vortex strength or circulation. Just as uniform flow and a doublet could be superposed to give non-lifting flow over a cylinder, the further superposition of a vortex gives lifting flow over a cylinder. This is the desired model, and its generation is shown in Figure 2 (Anderson, 1984: 156).

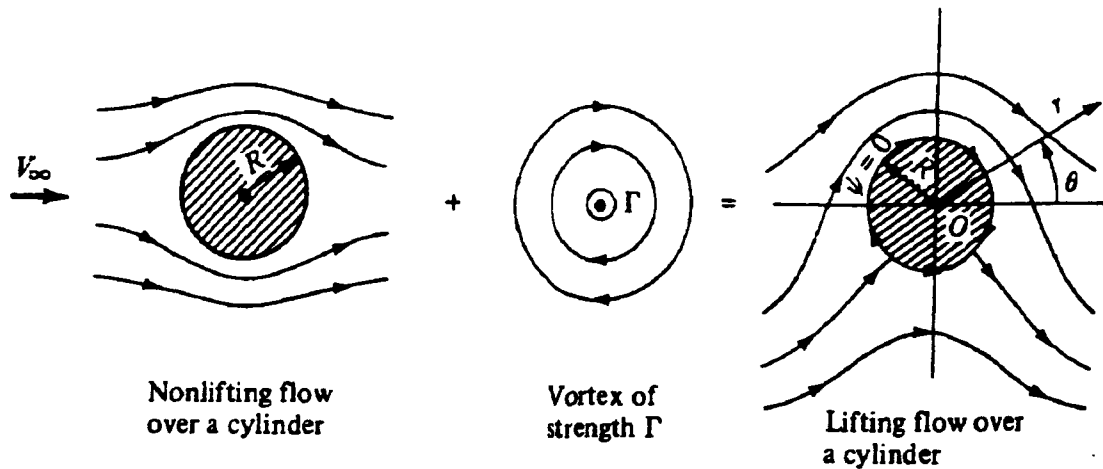


Figure 2. Superposition of Elementary Solutions for Lifting Flow over a Cylinder (Anderson, 1984: 156)

In this model created by the superposition of elementary flow solutions, the vortex strength is directly proportional to the rotation speed of the cylinder, and for a given freestream velocity, there are an infinite number of solutions corresponding to the infinite number of possible vortex strengths. One way in which the nature of the flow will be affected by changing vortex strengths is in the location of the stagnation points. For $\Gamma=0$, the stagnation points are at the front and back of the cylinder as seen by the flow, corresponding to $\theta=\pi$ and $\theta=0$, respectively. As the circulation increases, the stagnation points move down the cylinder until they eventually coincide and then move off the cylinder surface, as shown in Figure 3 (Kuethe and Chow, 1986: 81).

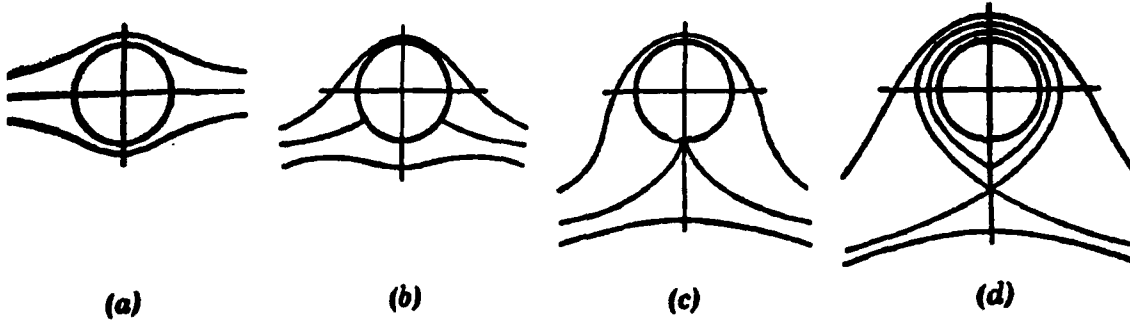


Figure 3. Migration of Stagnation Points for Different Values of Circulation: (a) $\Gamma = 0$, (b) $\Gamma < 4\pi V_\infty R$, (c) $\Gamma = 4\pi V_\infty R$, (d) $\Gamma > 4\pi V_\infty R$. (Kuethe and Chow, 1986: 81)

Knowing these solutions for the stream function allows the calculation of the velocity field, since

$$V_r = \frac{1}{r} \frac{\partial \psi}{\partial \theta} \quad (5)$$

and

$$V_\theta = -\frac{\partial \psi}{\partial r}. \quad (6)$$

The pressure coefficient is obtained as a function of angle θ as

$$c_p = 1 - \left[4 \sin^2 \theta + \frac{2\Gamma \sin \theta}{\pi r V_\infty} + \left(\frac{\Gamma}{2\pi r V_\infty} \right)^2 \right], \quad (7)$$

and from this the drag coefficient is predicted as

$$c_d = \frac{1}{2} \int_{\pi}^0 c_{p,upper} \cos \theta d\theta - \frac{1}{2} \int_{\pi}^{2\pi} c_{p,lower} \cos \theta d\theta. \quad (8)$$

The expression for pressure coefficient is the same on the upper and lower surfaces of the cylinder, so that the drag coefficient can be found in terms of a single integral,

$$c_d = -\frac{1}{2} \int_0^{2\pi} c_p \cos \theta d\theta. \quad (9)$$

Substituting the expression for pressure coefficient into this integral gives the incorrect result $c_d = 0$. This is known as d'Alembert's paradox, since he first published it in 1744.

(Anderson, 1984: 180)

Even though potential flow theory cannot predict drag, it gives useful information about the lift for flow over a rotating cylinder. The potential flow prediction for lift coefficient over an infinitely long rotating circular cylinder of radius R in a cross-flow is

$$c_l = \frac{\Gamma}{RV_\infty}, \quad (10)$$

and for the lift per unit span,

$$L' = \rho_\infty V_\infty \Gamma. \quad (11)$$

This result shows lift is directly proportional to circulation, and is known as the Kutta-Joukowski theorem. (Karamcheti, 1966: 388-389)

For tests involving rotating cylinders in a cross-flow, results for lift and drag may be presented in terms of a dimensionless parameter called the velocity ratio, α . This is defined as the ratio of the peripheral speed of the cylinder to the freestream speed,

$$\alpha = \frac{\omega_0 R}{V_\infty}. \quad (12)$$

In terms of the velocity ratio, the expression for the lift coefficient becomes

$$c_l = 2\pi\alpha \quad (13)$$

(White, 1979: 464).

Beyond Potential Flow

The shortcomings of basic potential flow theory, particularly its failure to predict drag on the cylinder, have lead to the formulation of more rigorous analyses. One of the most useful of these was developed by W. G. Bickley and later summarized by W. M. Swanson (Swanson, 1961: 461-470). In this analysis, an additional vortex besides the one in potential flow theory is included downstream of the cylinder, as shown in Figure 4. This additional vortex represents the shed vorticity in the cylinder's wake, and sets up an induced velocity field to produce an additional force beyond that due to the interaction of the freestream and the circulation within the cylinder body contour.

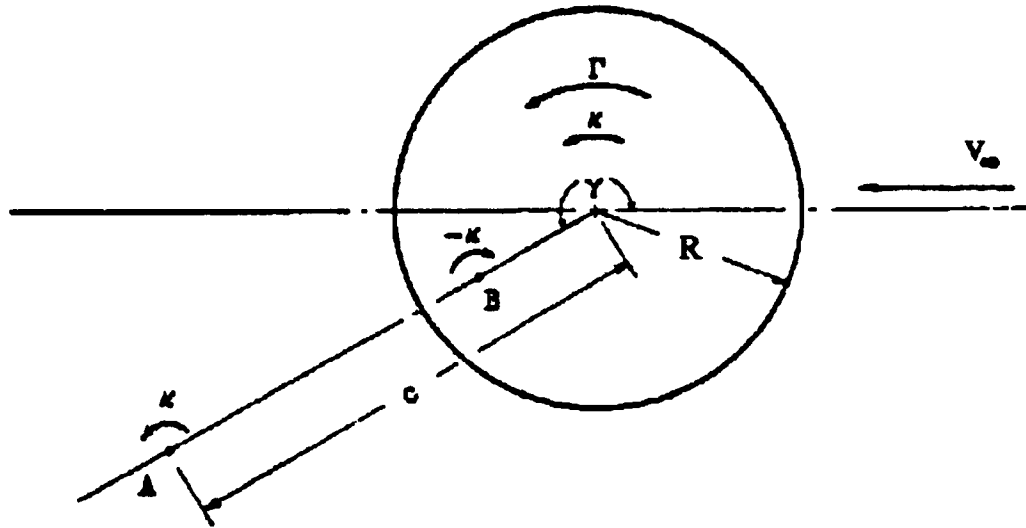


Figure 4. Shed Vortex Model (Swanson, 1961: 468)

The position of the shed vortex is specified by an angle relative to the freestream, called γ , and a radial distance, c . The predicted lift and drag coefficients depend not only on the angle γ and the ratio of the radial distance to the shed vortex and the radius of the cylinder, c/R , but also on a parameter K_a , which may be referred to as the Kutta-Joukowski coefficient. This parameter indicates the relative efficiency of the vortices, and would have a value of 2π in the ideal potential flow case, but must be less than this value to model actual flow phenomena more closely. With these definitions, the results from this analysis for the lift and drag coefficients are (Swanson, 1961: 468)

$$c_l = \left[1 - \left(\frac{R}{c} \right)^2 \right] K_a \alpha + \frac{\sin \gamma}{2\pi} \left(\frac{R}{c} \right) (K_a \alpha)^2 \quad (14)$$

and

$$c_d = -\frac{\cos \gamma}{2\pi} \left(\frac{R}{c} \right) (K_a \alpha)^2 \quad (15).$$

This model is capable of closely approximating some actual flow conditions; however, it requires knowing the functional relationships

$$\frac{R}{c} = \frac{R}{c}(\alpha), \quad (16)$$

$$\gamma = \gamma(\alpha) , \text{ and} \quad (17)$$

$$K_a = K_a(\alpha). \quad (18)$$

Unfortunately, these relationships must be determined empirically. This was done for previous tests with a single cylinder, and the parameters were found to have values of $\frac{R}{c} = 0.25$, $\gamma = 224^\circ$, and $K_a \alpha = 2.89$ (Swanson, 1961: 469). The lift and drag predicted by this model are included in the *Results* section.

Viscous Flow

As noted before, the prediction of zero drag in basic potential flow theory is a result of the assumption of inviscid flow. The actual flow around rotating cylinders is influenced by viscous effects. The problem of predicting the lift and drag forces on such rotating bodies in viscous flow fields has received much attention. Initially, this attention came in the form of a search for analytical solutions (for example, Wood, 1956: 77; Glauert, 1956: 89; and Moore, 1957: 541). Later, as computers became more powerful and computational fluid dynamics became more popular, emphasis shifted from analytical to numerical solutions (for example, Fornberg, 1985: 297; Badr and Dennis, 1985: 447; and Ingham and Tang, 1990: 91).

However, experimental data have been required to achieve the final desired results. The reason is noted by W. M. Swanson in a survey of investigations into this problem of analyzing the flow around rotating cylinders: "The formulation and solution of the mathematical problem is of sufficient difficulty that experimental results give the only reliable information on the phenomenon." (Swanson, 1961: 461)

This is still the case for the problem being investigated in this project. In fact, while computational solutions have improved, they have been limited to very low Reynolds numbers. As recently as 1985, the highest Reynolds number for which solutions

for viscous flow past a rotating cylinder had been obtained was 600 (Fornberg, 1985: 297).

III. Experimental Apparatus

Wind Tunnel

The experimental research for this project was done in an Aerolab educational wind tunnel in Building 640, Area B, Wright-Patterson AFB. A schematic drawing of this tunnel is included in Figure 5.

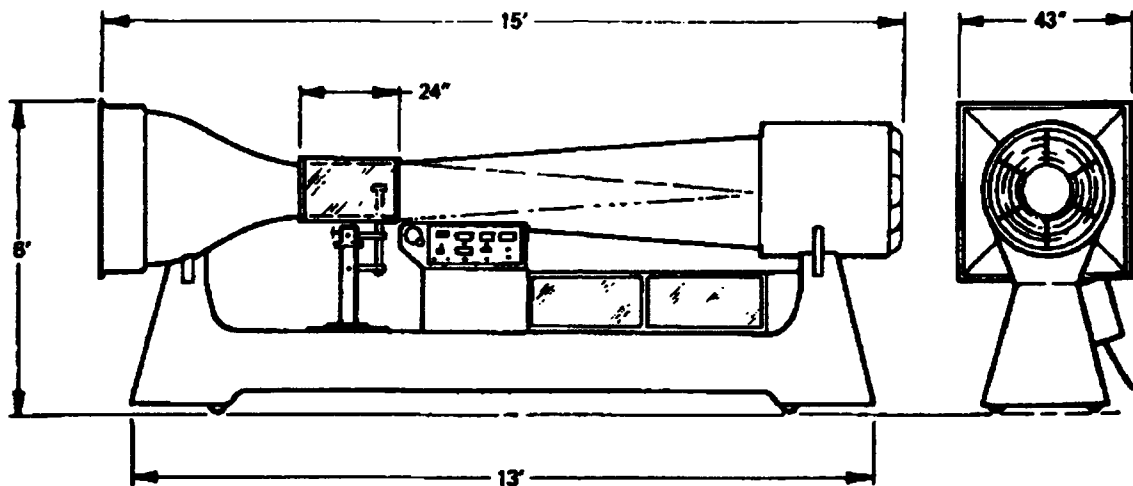


Figure 4. Aerolab Wind Tunnel Schematic

The test section was 12 inches by 12 inches in this fan-driven, open circuit tunnel. Airspeed in the tunnel was infinitely variable between 0 and 145 miles per hour, powered by a 10 horsepower drive motor with a variable frequency system. The entrance section of the tunnel held an aluminum honeycomb and two anti-turbulence screens, which kept the turbulence in the test section below 0.25%. (This figure was claimed by Aerolab, and was supported by tests conducted in the tunnel by a group of AFIT students in an experimental procedures course.)

Static pressure measurements were available from an orifice ring around the upstream end of the test section, and these pressures were used as the throat Venturi pressures in the tunnel's calculations of airspeed. The tunnel also had a sting balance on a turntable, as well as built-in force measurements and displays, but the sting was removed for this project due to the nature of the model setup.

Models

The models for these experiments were two 1-inch diameter aluminum cylinders mounted on a common support shaft via four sets of bearings. The support shaft had a diameter of 0.375 inches, chosen to accommodate the high-speed bearings. Each cylinder was 8.25 inches long, as shown in Figure 6.

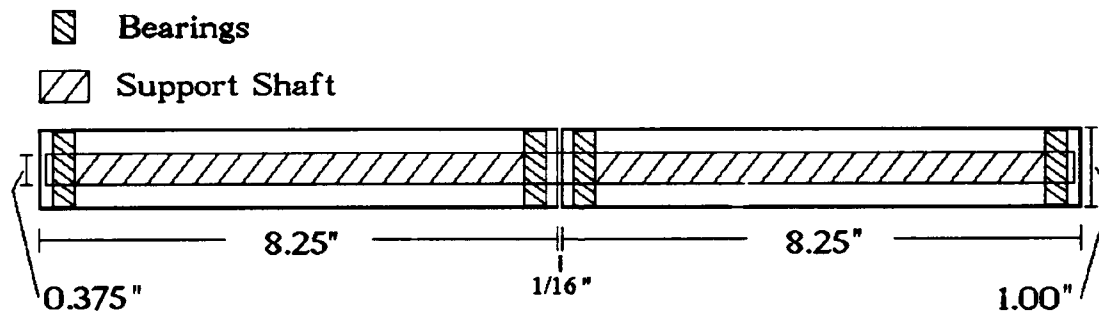


Figure 6. Cylinders on Support Shaft

The cylinders were mounted in the tunnel sidewalls in two different configurations. The primary configuration was for a direct cross-flow over the cylinders, as in Figure 7.

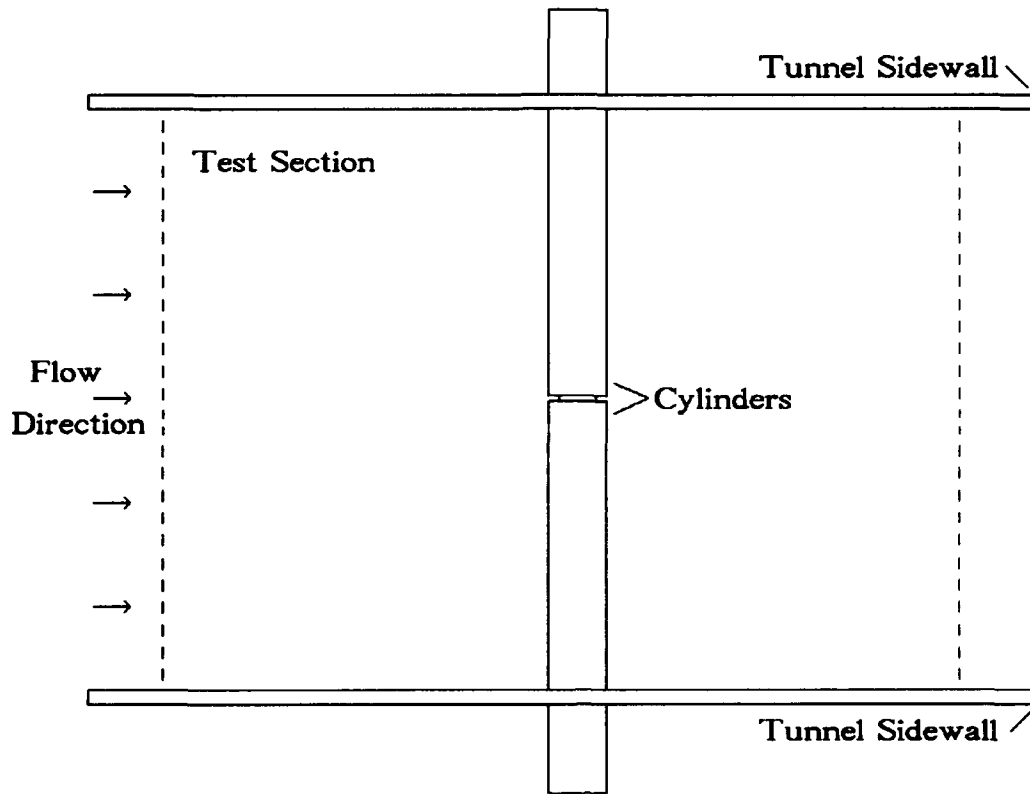


Figure 7. Primary Configuration of Cylinders in Wind Tunnel

The secondary configuration was 30° off from direct cross-flow, and is shown in Figure 8. For both configurations, special tunnel sidewalls were constructed, with holes to accommodate the cylinders, the bearings around the outside of the cylinders, and the spoke rings around the bearings.

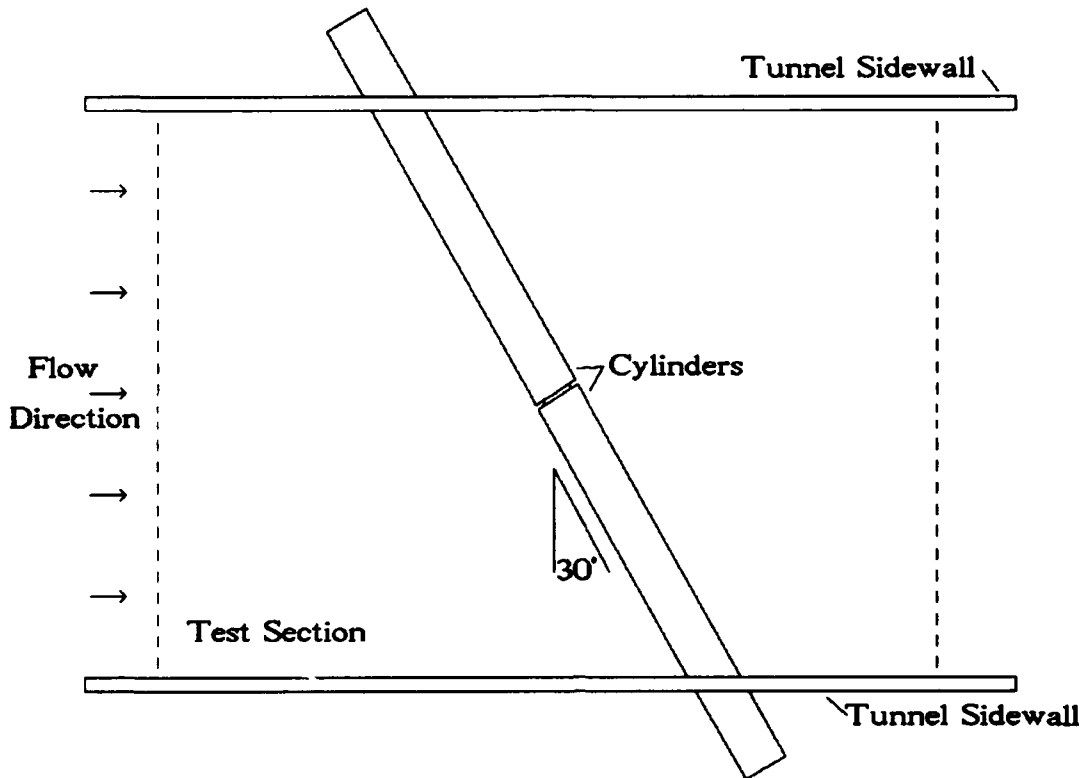


Figure 8. Secondary Configuration of Cylinders in Wind Tunnel

The spoke rings were key to force measurement, and will be discussed in the next subsection. A side view of the cylinders, bearings, and spokes is shown in Figure 9. The bearings outside the cylinders were high speed, angular contact ball bearings with a 1.0625-inch bore and a 1.3125-inch outer diameter. Since the cylinders were only 1.00 inches in diameter, a sheath was wrapped around them at the point where the bearings were mounted for a tight fit.

Assembly Dimensions:

Inner Diameter = 1.3125"

Outer Diameter = 2.325"

Width of Assembly = 0.25"

Spokes Dimensions:

Length (from inner ring to
outer ring) = 0.40625"

Width = 0.25"

Thickness = 0.05"

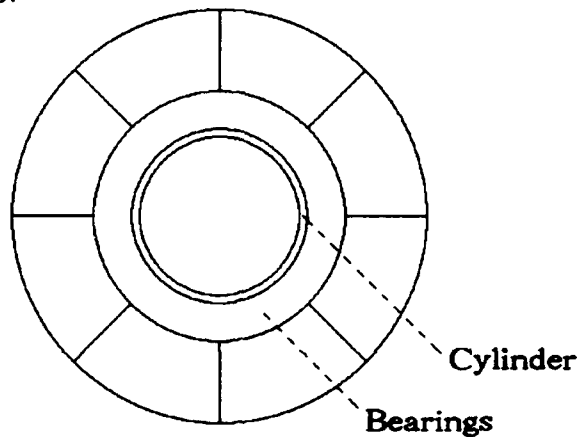


Figure 9. Side View of Spokes Assembly, Bearings, and Cylinder

Both cylinders were driven by Teledyne-Hanau air-powered dental drills, rated for approximately 30,000 rpm. These were chosen for several reasons. First, they were smooth-running and had reasonably high torque. A higher speed drill (380,000 rpm) was tried also, but it did not have enough torque to turn the cylinders. A direct-current motor for radio controlled race cars was also tried, but proved to be too rough-running, causing unacceptable noise in the data. Second, these drills were reversible, which gave them the best flexibility for changing the relative angular velocity of one cylinder to the other. The interface between these drills and the cylinders is shown in Figure 10.

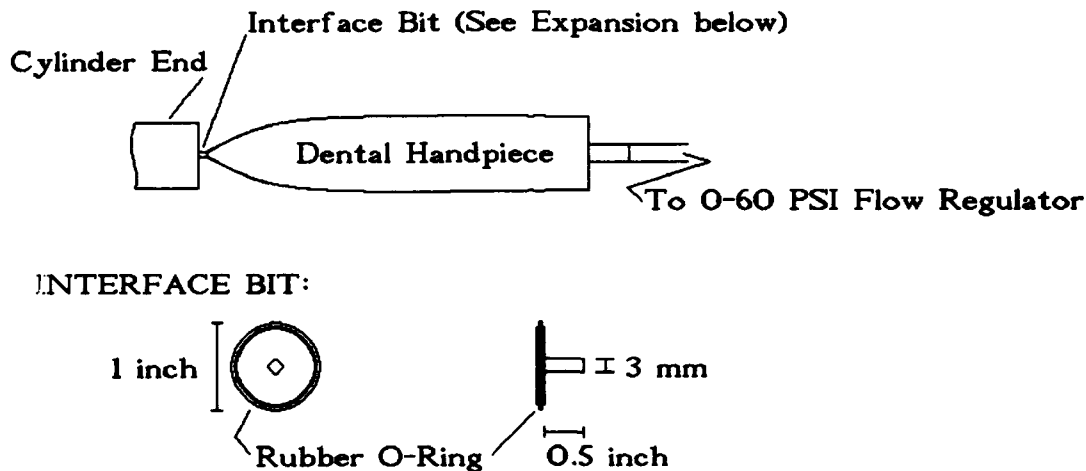


Figure 10. Cylinder/Drive Interface

Measurement Devices and Instrumentation

The fact that the cylinders were to rotate and be mounted in the tunnel to establish cross-flow precluded the use of a conventional sting balance and related force measurement devices. The way the cylinders were to be supported by the tunnel sidewalls lead to the decision to create a ring of spokes for each wall to facilitate the measurement of the necessary forces. Each ring had eight spokes, onto which were mounted strain gages on either side. A total of 32 Micro-Measurements general-purpose precision strain gages, each with a normal operating resistance of 120.0 ohms, were attached to the spokes.

The strain gages were connected to an amplifier and data acquisition system, as shown in Figure 11. This system included ten Pacific Instruments model 9355Q transducer amplifiers, connected via a General Purpose Interface Bus (GPIB) and IEEE-488 bus to an AT-class personal computer. The control and setup of the amplifiers was accomplished with software provided by the manufacturer. Four full bridge circuits from the strain gages on the spoke rings were connected to four amplifiers. These were for the

left and right side vertical and horizontal force measurements on the cylinders, corresponding with lift and drag, respectively. For each circuit, the excitation voltage was set to one volt, and the gain to 5000. These values were chosen due to the type of strain gage, and the need for sensitivity in the force measurements.

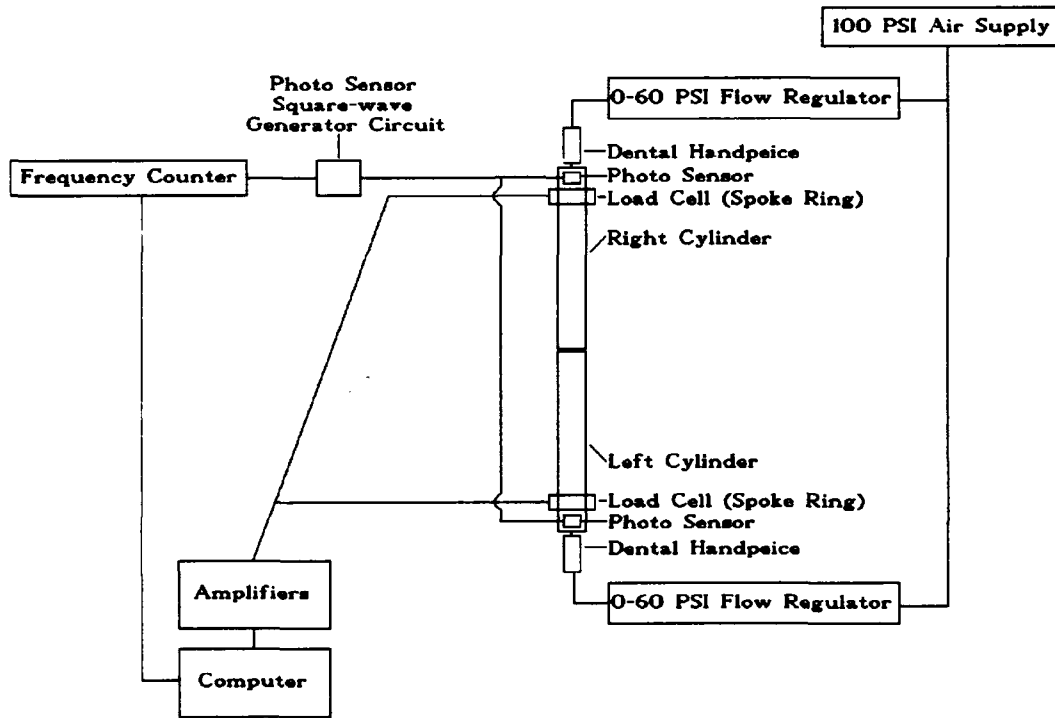


Figure 11. Experimental Setup Schematic

Another control parameter for the amplifiers was the filter frequency. Initially, tests were conducted with this set at the default value of 1000 Hz. However, noise in the data due to slight asymmetries in the rotation of the outer bearings lead to the selection of a lower frequency for the filters of 10 Hz. This improved the consistency and repeatability of the data.

To determine the angular velocities of the cylinders, an opaque stripe of paint was put on each cylinder, immediately outside the tunnel sidewalls, which caused photo-

sensitive devices (TRW type OPB707) placed directly above those areas of the cylinders to effectively generate a square wave with a frequency matching the speed with which the cylinders rotated. This square wave signal was sent to a frequency counter, which was also connected to the personal computer. The accuracy of this system was verified by using a strobe to also determine the frequency of rotation and compare with that given by the photo sensors.

During tests, data were recorded and stored on computer disk via a BASIC program, written to communicate with the amplifiers and frequency counters, and record their outputs. This computer program is included in Appendix A.

IV. Experimental Procedures

Flow Visualization

With both cylinders rotating at the same angular velocity, the configuration of the cylinders in the wind tunnel was very close to modelling a single cylinder of infinite aspect ratio. That is, tests for which both cylinders rotated together were close to two-dimensional. This idea was tested by a flow visualization experiment. For this test, several drops of flow visualization oil were placed on the upper surface of both cylinders, which were secured outside the tunnel to prevent them spinning. The wind tunnel was run to above 30 m/s, beyond the range of the tests to be conducted for gathering lift and drag data, and photographs were taken of the oil drop patterns. One such photograph is included in the next chapter.

Strain Gage Calibrations

Before taking any data, the force measurement equipment and data acquisition system were calibrated. In this manner, the raw data gathered in the experiments could be translated into meaningful results.

The strain gages had to be calibrated for each of the two configurations used in this project. The results from each calibration and the specific configuration to which they were applied are included in the next chapter, but in each case the procedure for calibrating the gages was the same. A series of weights were attached by a thin wire to the cylinders. For calibrating the vertical force readings, these weights were allowed to hang freely beneath the cylinders, and output in millivolts corresponding to each individual load were gathered. To calibrate the horizontal force readings, a pulley with bearings was placed on the conventional sting balance mounting brace which came with the wind tunnel. The wire to hold the weights was draped over this pulley to cause the full force of the weight to be felt in the drag direction from the cylinders' perspective.

In these calibrations, the cylinders on their common support shaft were treated as a beam supported at both ends, with a point load on it. Since there was a spoke ring or load cell on each end at the point of support, the sum of the two forces predicted by the load cells equalled the total force on the cylinders. This was the case whether the load was centered along the span of the cylinders or not. However, to treat the distributed load on the cylinders in this manner, the interaction coefficients between the two load cells were ignored. That is, when a force was applied at one load cell, any slight effect at the other cell was neglected.

To verify the accuracy of this type of calibration, check loads were applied to the cylinders, to which the force calculated with the calibrations were compared. Centered horizontal and vertical check loads were applied, as well as off-center vertical loads. It was found that the calibrations closely predicted the actual forces applied to the cylinders. The results of the calibrations and the check-load tests are in the next chapter.

Force Measurement Validity Check

To determine whether or not the setup was able to measure aerodynamic forces, a validity check was performed. This test involved running the wind tunnel through a range of freestream velocities without rotating the cylinders. The velocities ranged from 15.24 to 30.48 m/s, the same range of velocities for which spinning-cylinder tests would be run. The drag coefficients were calculated and plotted versus Reynolds number, and compared with predictions for a two-dimensional or infinite-span cylindrical cross-section.

Single Cylinder Tests

The initial tests conducted with the cylinders rotating were for a single cylinder. This was done to gather data for comparison with previous experiments, as a validation for the force measurement scheme and the test setup in general.

The range of velocity ratios (peripheral speed of the cylinder to freestream speed, $\alpha = \frac{\omega_0 R}{V_\infty}$) over which the tests were initially planned was about one to six. This had to be considerably limited as the project proceeded, due to the limitations on the rotation rates achieved. As mentioned in the preceeding chapter, several drive mechanisms were tried for spinning the cylinders. The drives that were finally used were 30,000 rpm reversible dental handpieces, which were smooth-running and had enough torque to get the cylinders spinning.

However, with both cylinders spinning on their common support shaft, resonant vibrations became noticeable above 8000 rpm. These vibrations increased in magnitude when the angular velocities were further increased, and did not seem to dissipate or smooth out. For this reason, the maximum angular rotation rate used in the tests for this project was 8000 rpm. With this limit on rotation rate, and with a lower limit on freestream velocity imposed to ensure measurable force levels on the cylinders, the maximum velocity ratio tested at was about 0.7.

The first step for testing with the cylinders rotating was to zero the airspeed indicator on the wind tunnel. This procedure was complicated by the fact that the wind tunnel's calculation of airspeed depended on an internal square root function, and could therefore not handle a negative number. As per the instructions given in the wind tunnel manual, a pressure was applied to the tunnel's pressure sensor until a positive airspeed was indicated, then the airspeed zeroing control was adjusted without that pressure applied until the airspeed indicator just read zero. This step generally only had to be done once each time the tunnel was powered on.

The next step in the single cylinder tests was to select the desired airspeed via the front panel control on the wind tunnel. Then the angular velocity was set for the cylinder

by adjusting the air pressure on the dental drills used to turn the cylinders, and monitoring the frequency on the counter.

Finally, with the aid of the data acquisition program, the key parameters were recorded for later analysis. These recorded parameters were the angular rotation rates of the cylinders, and the output voltage from each of the four bridge circuits on the spoke rings. Other data that were collected each day of testing were the ambient temperature and pressure, which were used to get density, coefficient of viscosity, and Reynolds number. The key parameters to come out of this data in the reduction process were the velocity ratio, α , the lift and drag on the cylinders, and the lift and drag coefficients.

Dual Cylinder Tests

The unique part of this project was the testing done with the cylinders rotating with different angular velocities. In these tests, the procedures for zeroing the airspeed, selecting the freestream velocity on the wind tunnel, and monitoring the outputs were the same as for the single cylinder tests. However, the selection and setting of angular velocities for the two cylinders was more complex.

The single-cylinder tests were used as the baseline. From this, one of the cylinders was set to a different rpm in increments of 20%, from -60% to +60% of the baseline angular rotation rate. The key data sought in these tests were the change in lift and drag coefficients on the cylinders. By noting these changes, it was sought to infer the possible effect one cylinder's change in angular velocity had on the system of two cylinders. The lift and drag coefficients for all of these tests were found by using the strain gage calibrations to find the forces of lift and drag on the cylinders, and non-dimensionalizing these by dividing by the dynamic pressure, cylinder diameter and length, as follows:

$$c_l = \frac{Lift}{\frac{1}{2} \rho V_{\infty}^2 (Diameter)(Length)}, \text{ and} \quad (19)$$

$$c_d = \frac{\text{Drag}}{\frac{1}{2} \rho V_{\infty}^2 (\text{Diameter})(\text{Length})}. \quad (20)$$

These computations for a specific test example are included in Appendix B.

Offset Tests

After the tests in direct cross-flow had been completed, the second set of wind tunnel sidewalls was mounted in the tunnel, which held the cylinders at an offset of 30° to direct cross-flow. In this configuration, tests were conducted with both cylinders spinning at the same angular velocity, to compare with the single cylinder tests in this project. The purpose for doing these offset tests was to determine if the cross-flow component, or normal component of velocity was the only factor in the forces of lift and drag on the cylinders. The wind tunnel velocities for these tests were chosen such that the normal component of velocity over the cylinders matched the velocities at which tests were conducted in the primary configuration. This normal component of velocity was substituted for freestream velocity, V_{∞} , in the force non-dimensionalization, equations 19 and 20. The procedures for these tests were the same as for the single-cylinder tests described above, with only the offset angle being different.

V. Results

Flow Visualization

The first test conducted was flow visualization. The purpose of this test was to determine how closely two-dimensional flow was being modeled by the experimental setup. Figure 12 shows the primary configuration in perspective as it was mounted in the wind tunnel. Once the tunnel velocity was taken above 30 m/s with the flow visualization droplets on the cylinders' upper surfaces, photographs were taken of the droplet patterns. One such photo is included as Figure 13. From this picture, it can be seen that there was very little tendency for the flow to try to go outside the span of the cylinders through the small gaps in the tunnel sidewalls to allow cylinder rotation. Thus, this setup very closely modeled two-dimensional flow.

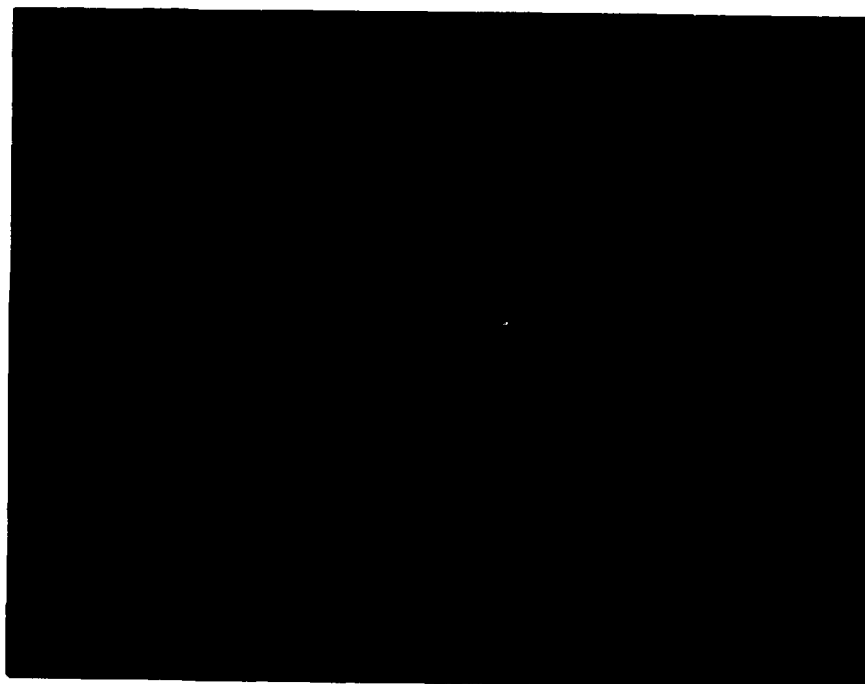


Figure 12. Cylinder Models in Primary Configuration

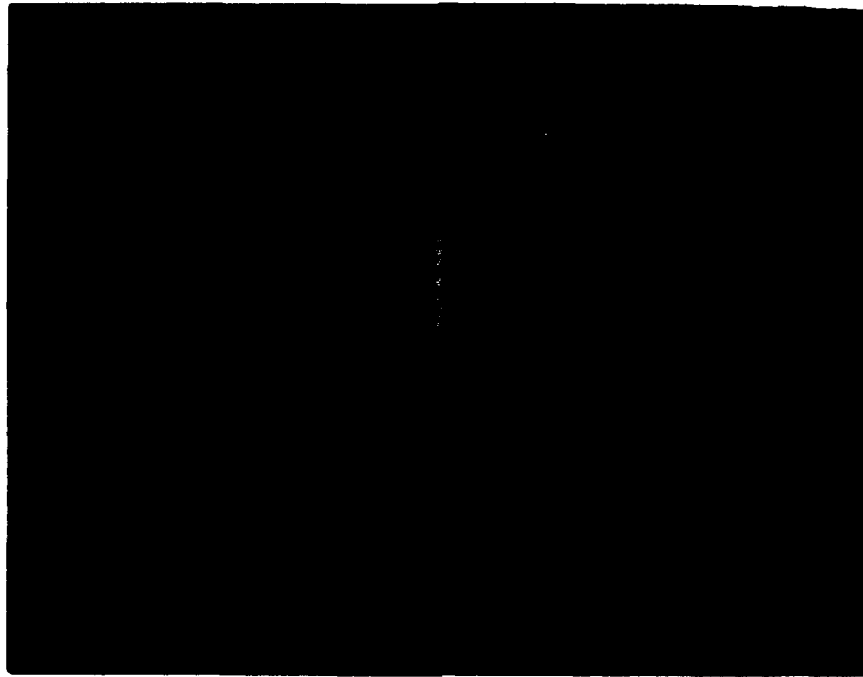


Figure 13. Results of Flow Visualization Test

Calibrations

As mentioned in the Experimental Procedures section, calibrations were performed on the strain gages for both the primary and secondary configurations. Static check loads were applied to test the accuracy of these calibrations.

Primary Configuration

The primary configuration, with the cylinders normal to the freestream flow, was calibrated first. The results for the left and right load cells, for both the vertical and horizontal directions, are shown in Figures 14 through 17. All of these calibration curves were found to be linear, as was expected for the strain gages. The negative slope on the left horizontal calibration was a result of the way the bridge of four strain gages for that

direction were wired and connected to the amplifier system. This different sign posed no problem, as the calibrations were all applied to the collected test data in the same way.

Secondary Configuration

When the second set of tunnel sidewalls were installed, with the cylinders offset from direct crossflow by 30° , the strain gages were recalibrated. One of the load cells was damaged in the transition between configurations, and so different strain gages were wired to provide the vertical and horizontal bridges on the left side. Curiously, the left horizontal bridge was more sensitive than the others when it was rewired. A possible explanation for this is that the pair of spokes used for that bridge may have been slightly thinner than the others. This left horizontal bridge was also rewired in the same orientation as the others, so that its slope was also positive. Neither this nor its increased sensitivity had any ultimate consequence once the calibration curve fits were applied to the test data.

The secondary configuration calibration results are shown in Figures 18 through 21. The tabulated data for the calibrations are in Appendix C.

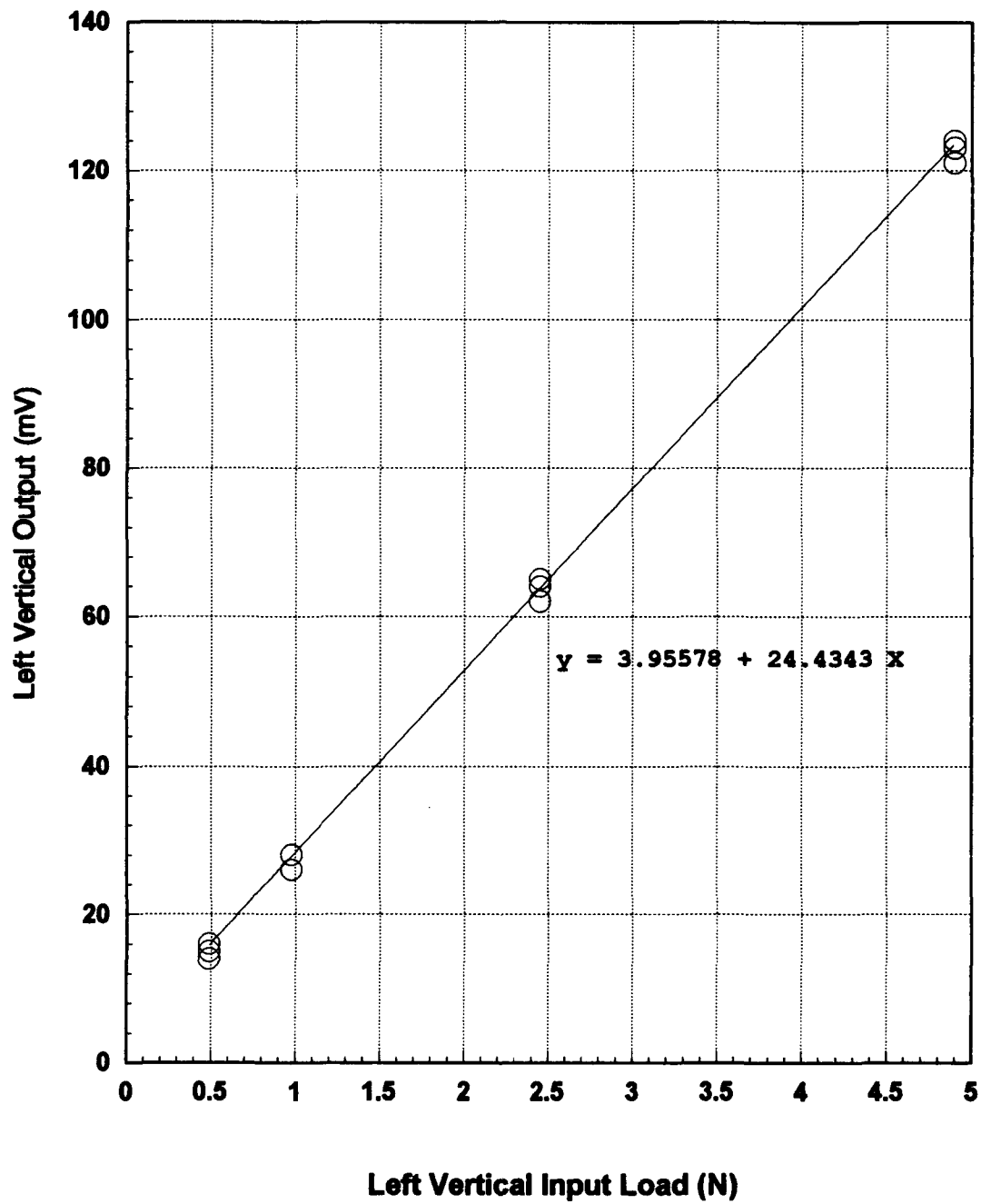


Figure 14. Left Vertical Bridge Calibration for Primary Configuration

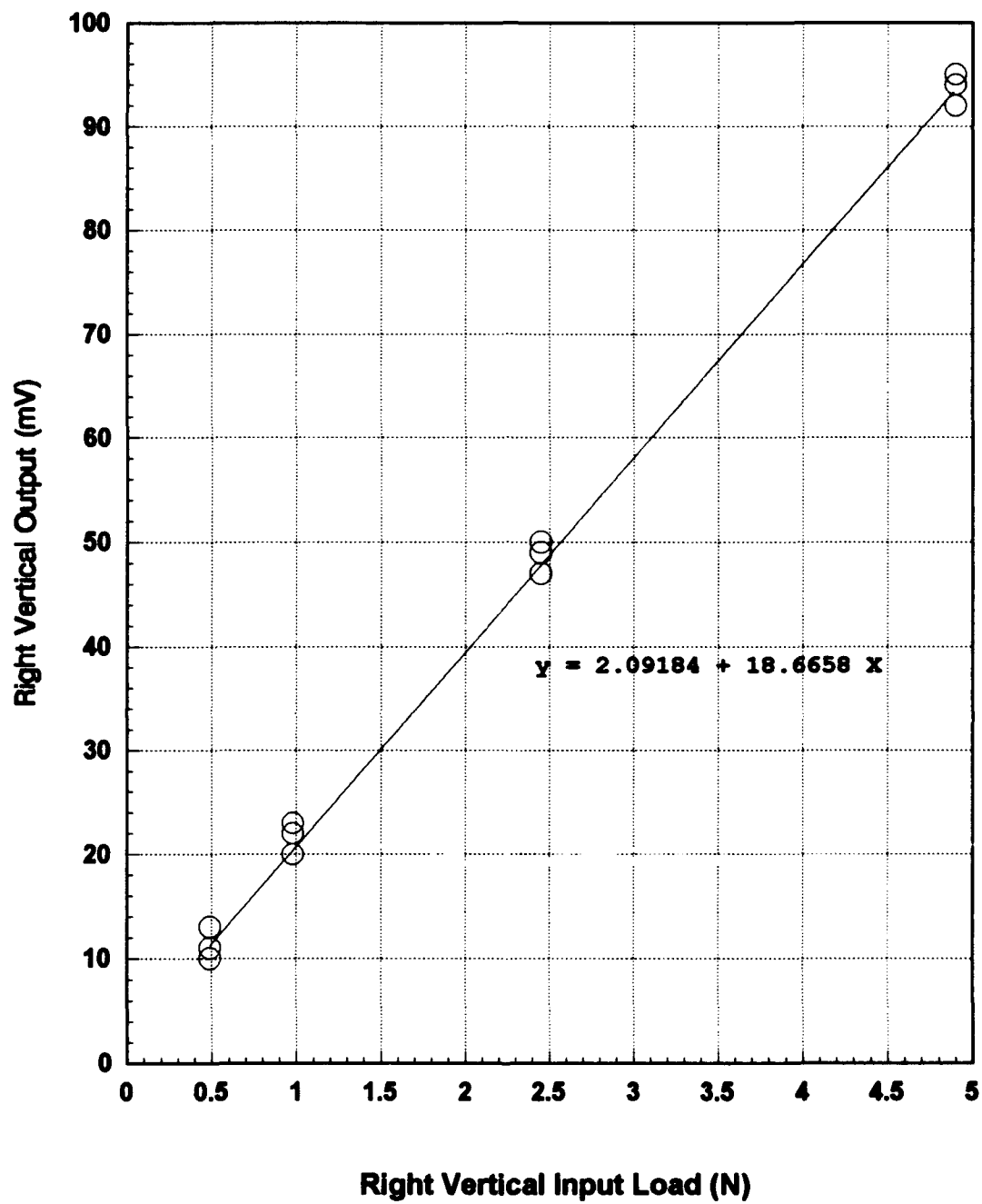


Figure 15. Right Vertical Bridge Calibration for Primary Configuration

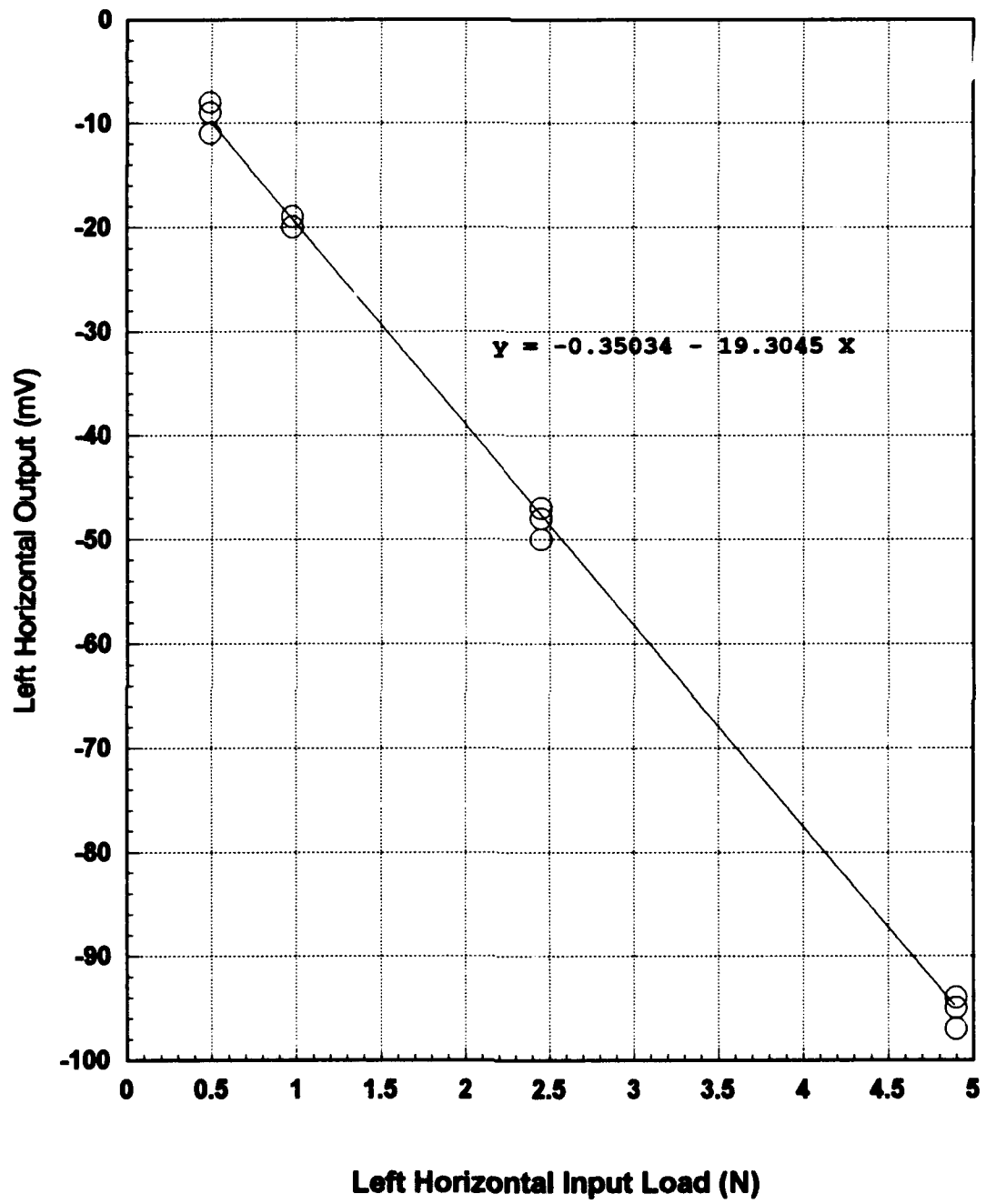


Figure 16. Left Horizontal Bridge Calibration for Primary Configuration

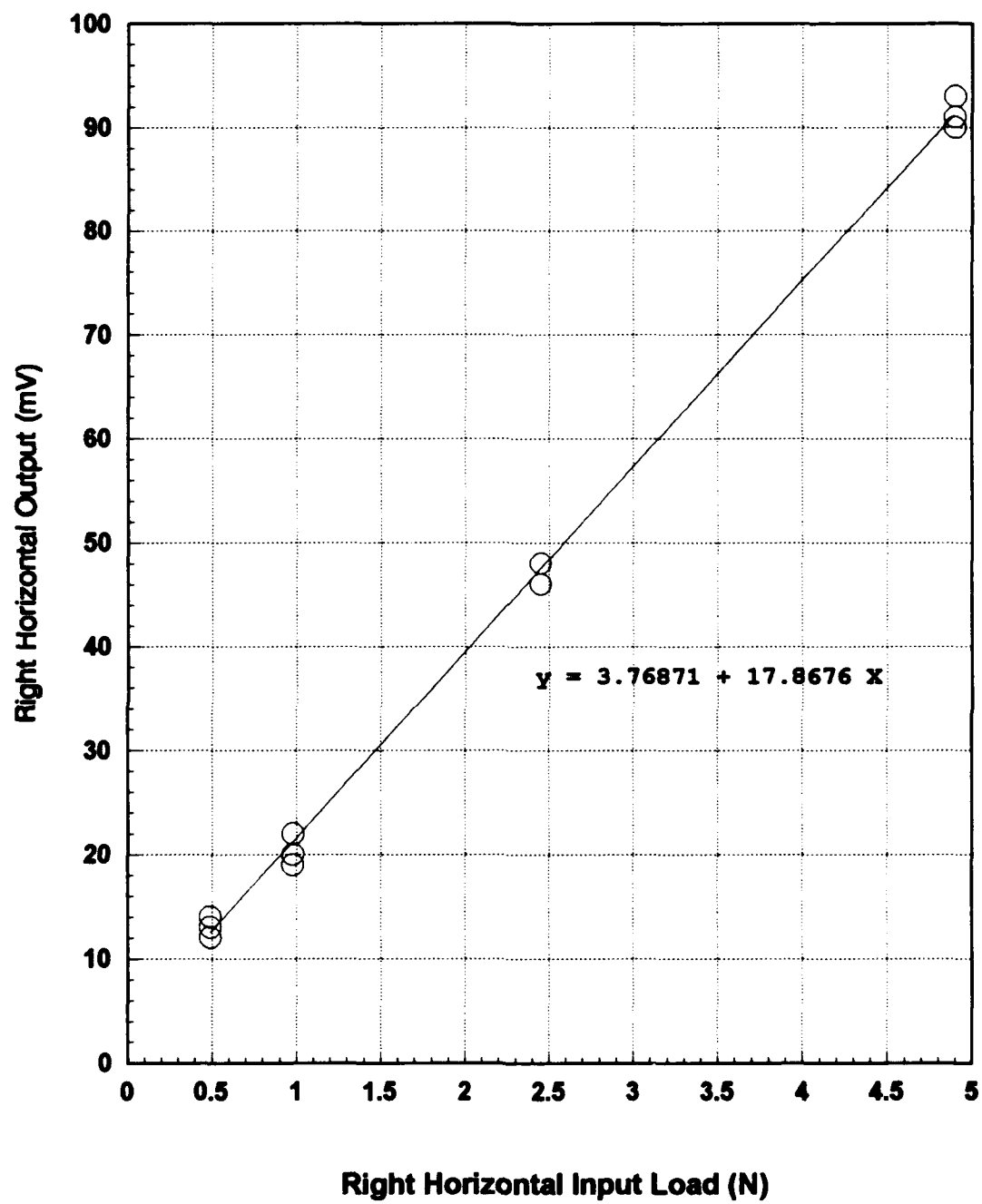


Figure 17. Right Horizontal Bridge Calibration for Primary Configuration

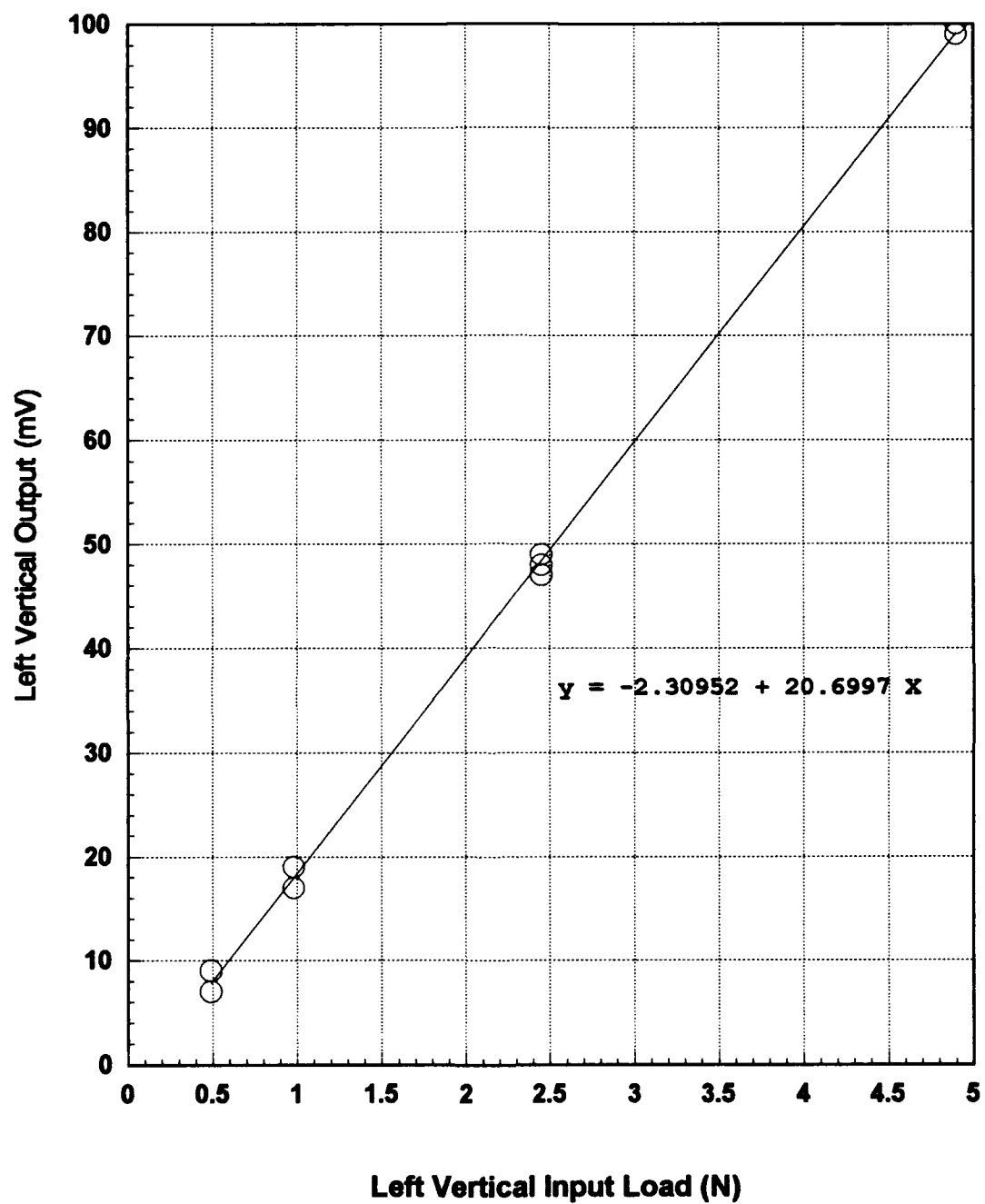


Figure 18. Left Vertical Bridge Calibration for Secondary Configuration

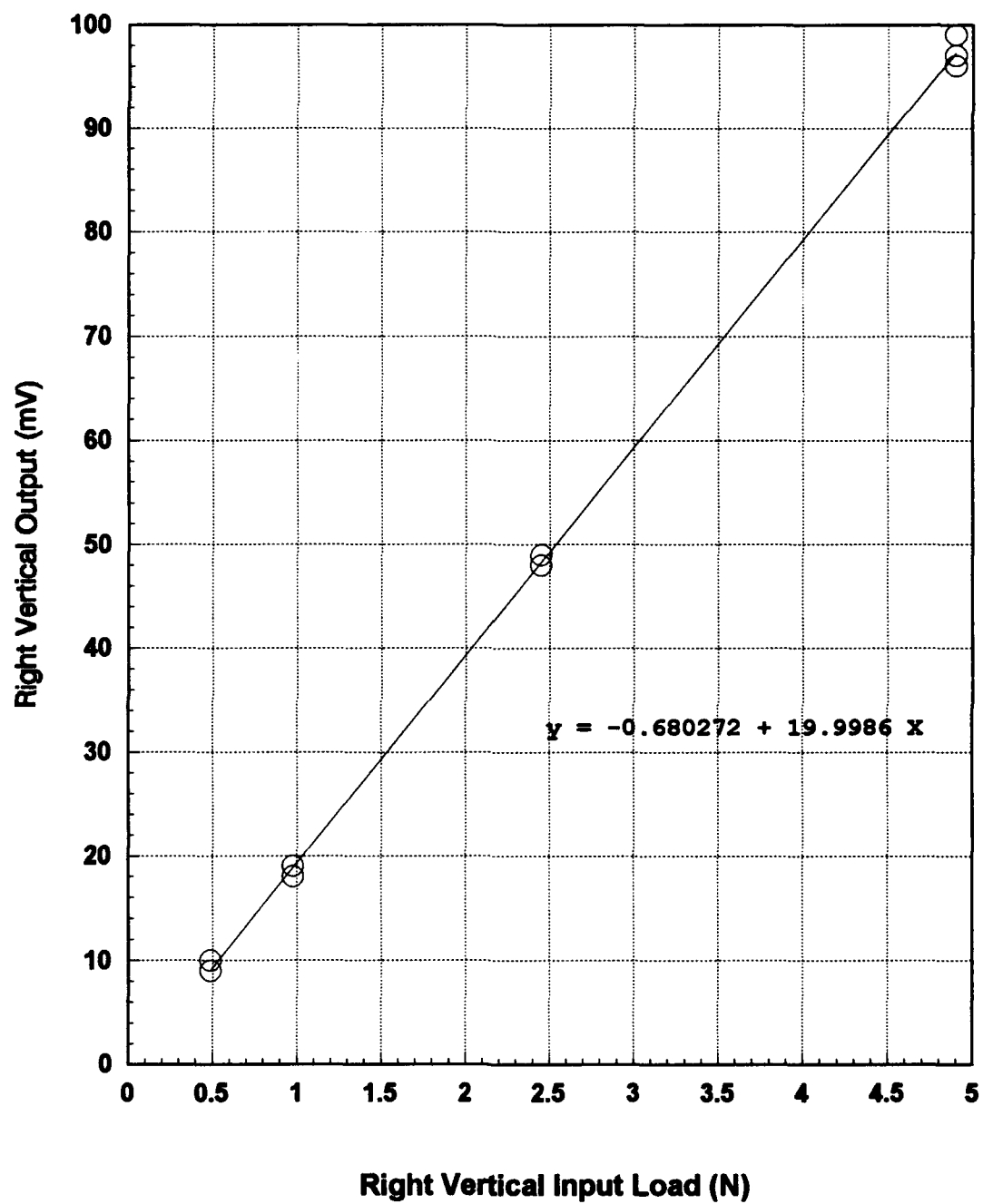


Figure 19. Right Vertical Bridge Calibration for Secondary Configuration

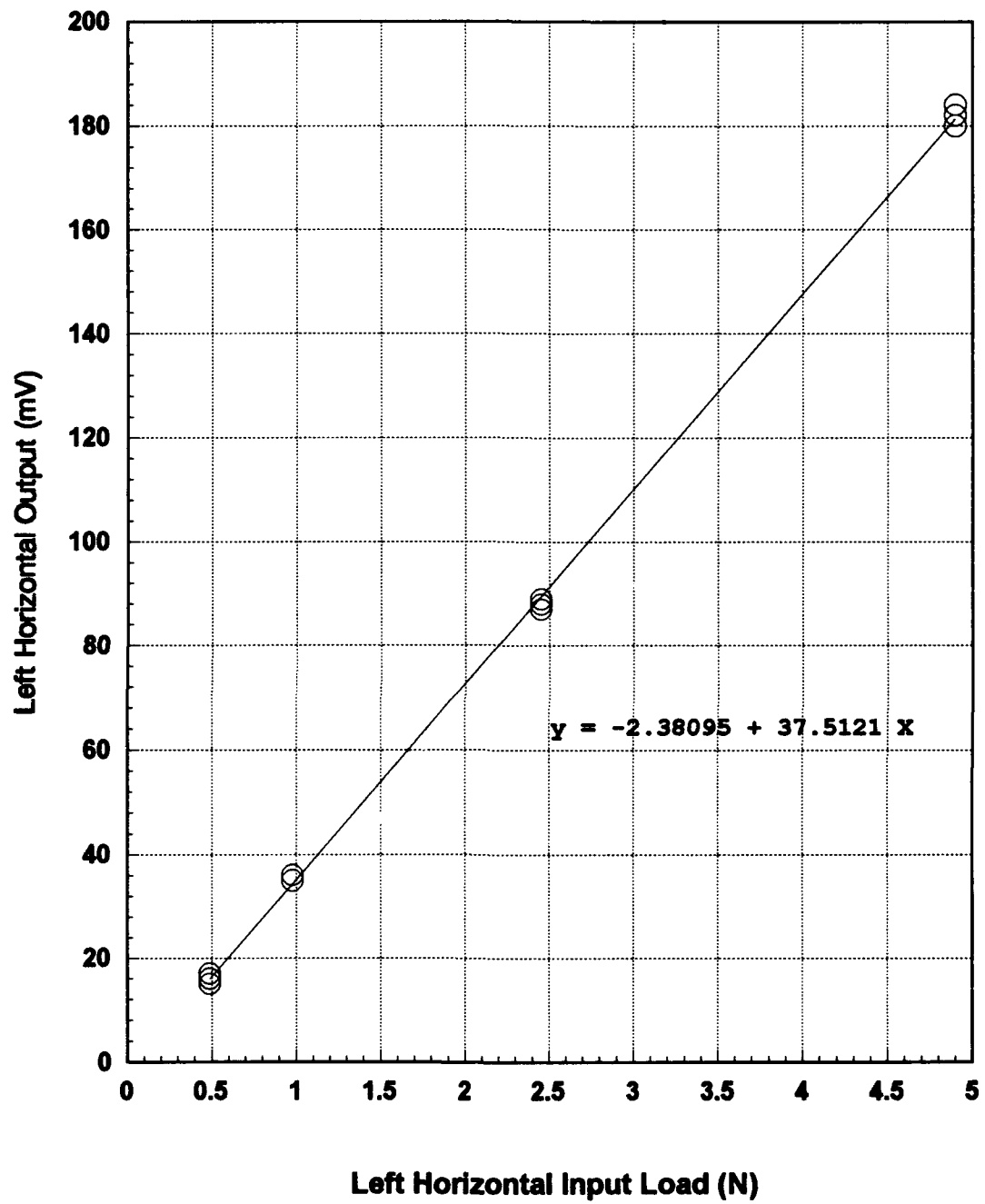


Figure 20. Left Horizontal Bridge Calibration for Secondary Configuration

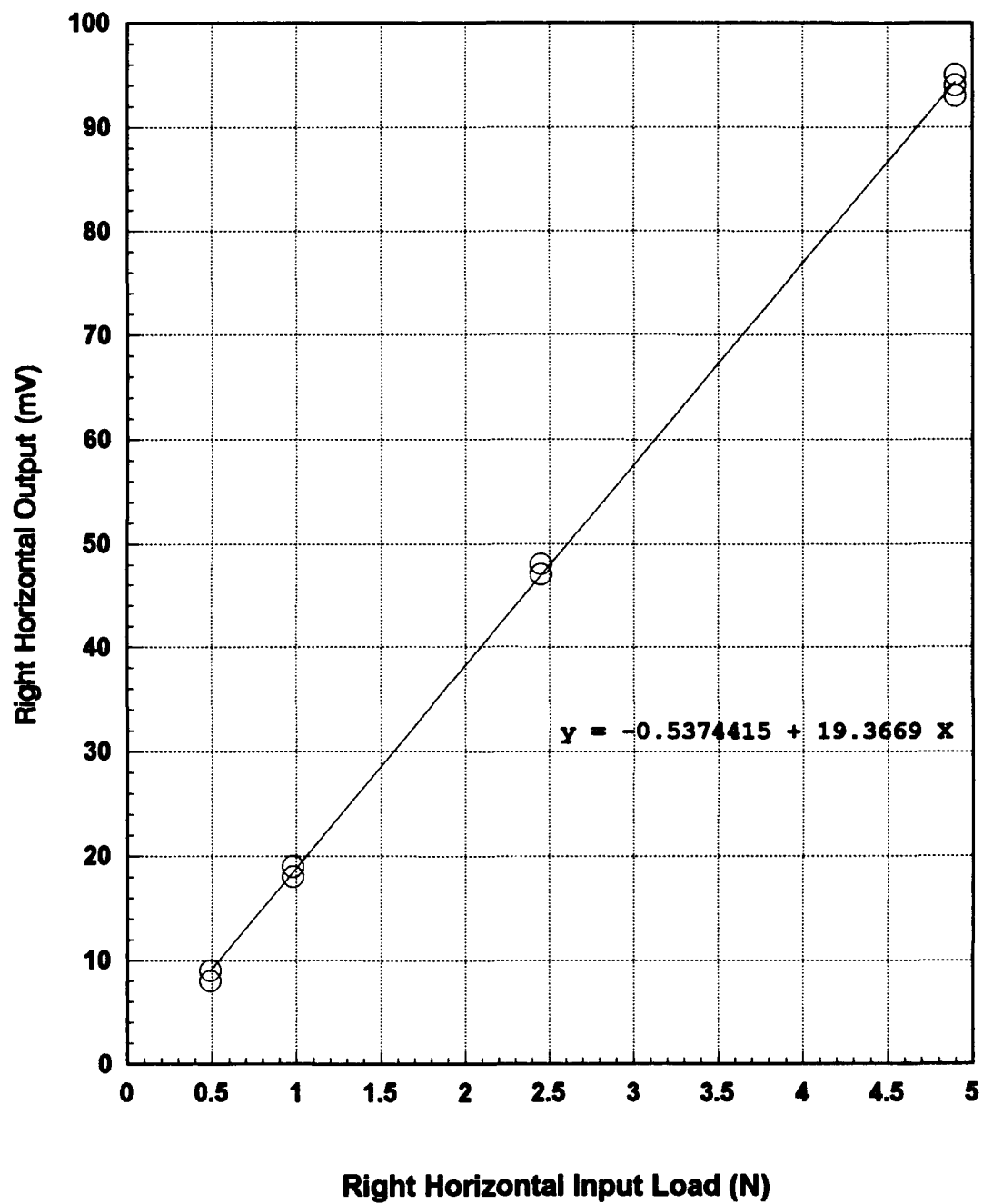


Figure 21. Right Horizontal Bridge Calibration for Secondary Configuration

Check Loads

To verify the calibrations, static check loads were applied to the cylinders. Horizontal centered loads, vertical centered loads, and off-center vertical loads were applied to the cylinders in the primary configuration. The calibrations were applied to the output data, and these calculated loads were compared to the actual applied loads. The results of these tests are in Tables I to III. These results show that the load cells with their calibrations were capable of accurately indicating (within an average of 1.37%, with a maximum error of 3.67%) static forces on the cylinders.

TABLE I.
Centered Vertical Check Loads.

Total Mass Applied (kg)	Total Force Applied (N)	Left Vertical Output (mV)	Right Vertical Output (mV)	Total Force Calculated (N)
0.2	1.96	28	21	1.99
0.5	4.9	63	45	4.72
0.7	6.86	90	64	6.84

TABLE II.
Centered Horizontal Check Loads.

Total Mass Applied (kg)	Total Force Applied (N)	Left Horizontal Output (mV)	Right Horiz. Output (mV)	Total Force Calculated (N)
0.2	1.96	-19	21	1.93
0.5	4.9	-48	46	4.83
0.7	6.86	-63	64	6.82

TABLE III.
Off-Center Vertical Check Loads.

Total Mass Applied (kg)	Total Force Applied (N)	Left Vertical Output (mV)	Right Vertical Output (mV)	Total Force Calculated (N)
0.2	1.96	19	27	1.95
0.5	4.9	41	63	4.79
0.7	6.86	66	82	6.82

Force Measurement Validity Check

Another set of tests was conducted to give confidence in the data gathered from this experimental setup. These tests involved a sweep of freestream velocities over the non-rotating cylinders, with the intention of finding the drag coefficient versus Reynolds number. The velocities tested were from 15.24 to 30.48 m/s, which were the same as for the rotating cylinder tests. Ambient temperature and atmospheric pressure were measured and used to calculate the density based on the assumption of a perfect gas:

$$\rho = \frac{P}{RT}, \quad (17)$$

where R is 287 J/(kg)(K). The coefficient of viscosity was calculated via Sutherland's equation for air,

$$\frac{\mu}{\mu_0} = \left(\frac{T}{273K} \right)^{\frac{3}{2}} \frac{273K + 111K}{T + 111K}, \quad (18)$$

where $\mu_0 = 1.716 \times 10^{-5} \text{ N s/m}^2$ (White, 1990: 28). From these, the Reynold's number was calculated as

$$\text{Re} = \frac{\rho D V_{\infty}}{\mu}. \quad (19)$$

For these tests in the primary configuration, the conditions were as follows: $T = 293K$, $p = 98189 \text{ N/m}^2$, $\rho = 1.17 \text{ kg/m}^3$, and $\mu = 1.814 \times 10^{-5} \text{ N sec/m}^2$. In the secondary configuration, $T = 295K$, $p = 98358 \text{ N/m}^2$, $\rho = 1.16 \text{ kg/m}^3$, and $\mu = 1.823 \times 10^{-5} \text{ N sec/m}^2$. The results of these tests for each configuration are shown in Figure 22. Along with these data are shown previous results for an infinite cylinder (White, 1991: 11), and for a finite cylinder with an aspect ratio of five (Breuer, 1983: 2-26). The data collected in this project fall between $24000 < \text{Re} < 50000$, which is about where a sharp reduction in drag is predicted for a roughened cylinder in White's data. The cylinders in this test were neither intentionally roughened nor of infinite span; however, the

flow visualization tests revealed that this setup closely approximated two-dimensional flow, which would be the case for an infinite span cylinder. Therefore, the trend in the test data for a reduction in drag over this range of Reynolds number should not be surprising.

These tests showed that the experimental setup with its load cells of strain gages on spoke rings was able to measure aerodynamic loads. Further, the close correlation between the data from the primary and secondary configurations gave a clear indication that the normal component of the freestream velocity was the important component to be considered, at least to the offset angle tested, 30° . Note that the tests in the secondary configuration were at higher freestream velocities such that the normal component of velocity over the cylinders matched that in the tests in the primary configuration. The data in tabular form are included in Appendix C.

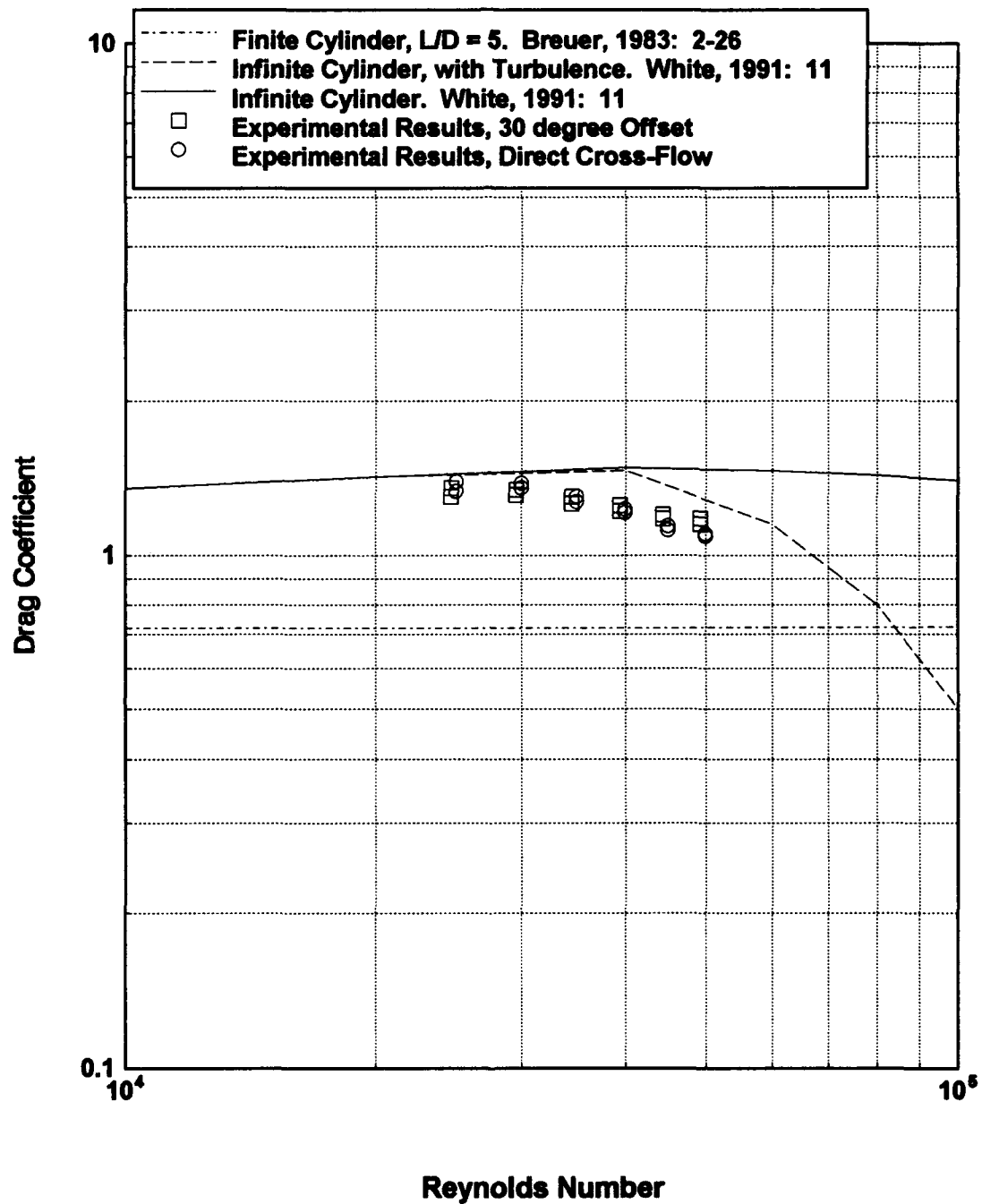


Figure 22. Drag Coefficient Versus Reynolds Number

Single Cylinder Tests

The first tests with the cylinders rotating were in the primary configuration with both cylinders rotating at the same rate, to simulate a single cylinder. These tests were done to get a baseline of data which could be compared with previous single cylinder tests, and with which the tests with the two cylinders rotating at different rates could be compared. The lift coefficient data are presented in Figure 23, and the drag coefficient data in Figure 24. The line plotted as experimental results represents a second-order regression of the data. The actual data had fluctuations, or noise, ranging up to about $\pm 15\%$. This noise was examined with an oscilloscope, and was determined to most likely be caused by non-uniform rotation of the bearings within the load cells. It was found that using a lower frequency filter of 10 Hz, as opposed to the 1000 Hz filter which was being used on the strain gage amplifiers, considerably reduced the noise (to a worst case of about $\pm 7.5\%$) without changing the trends in the data. All these data are included in Appendix C, Tables VIII and IX.

The lift coefficient data falls considerably above that from Thom in 1934 (Swanson, 1961: 462), but is much closer to the data from White (White, 1979:464), as shown in Figure 25. The potential flow theory is much too high, but the shed vortex theory predictions are fairly reasonable. The drag coefficient data, shown in Figure 26, is also fairly close to White's, but is somewhat different from either extrapolation offered by Swanson for his 1961 data (Swanson, 1961: 465). Both of Swanson's extrapolations are from the same experimental data, indicating some uncertainty about what occurred below the range of velocity ratios at which he tested. Because of the limited range of velocity ratios in this project, predicting whether a sharp decrease in the drag coefficient would occur before the ensuing drag rise at higher velocity ratios was not possible. The shed vortex theory, while it overcomes the zero drag dilemma of strict potential flow theory, does not accurately predict the drag at velocity ratios below about 1.5.

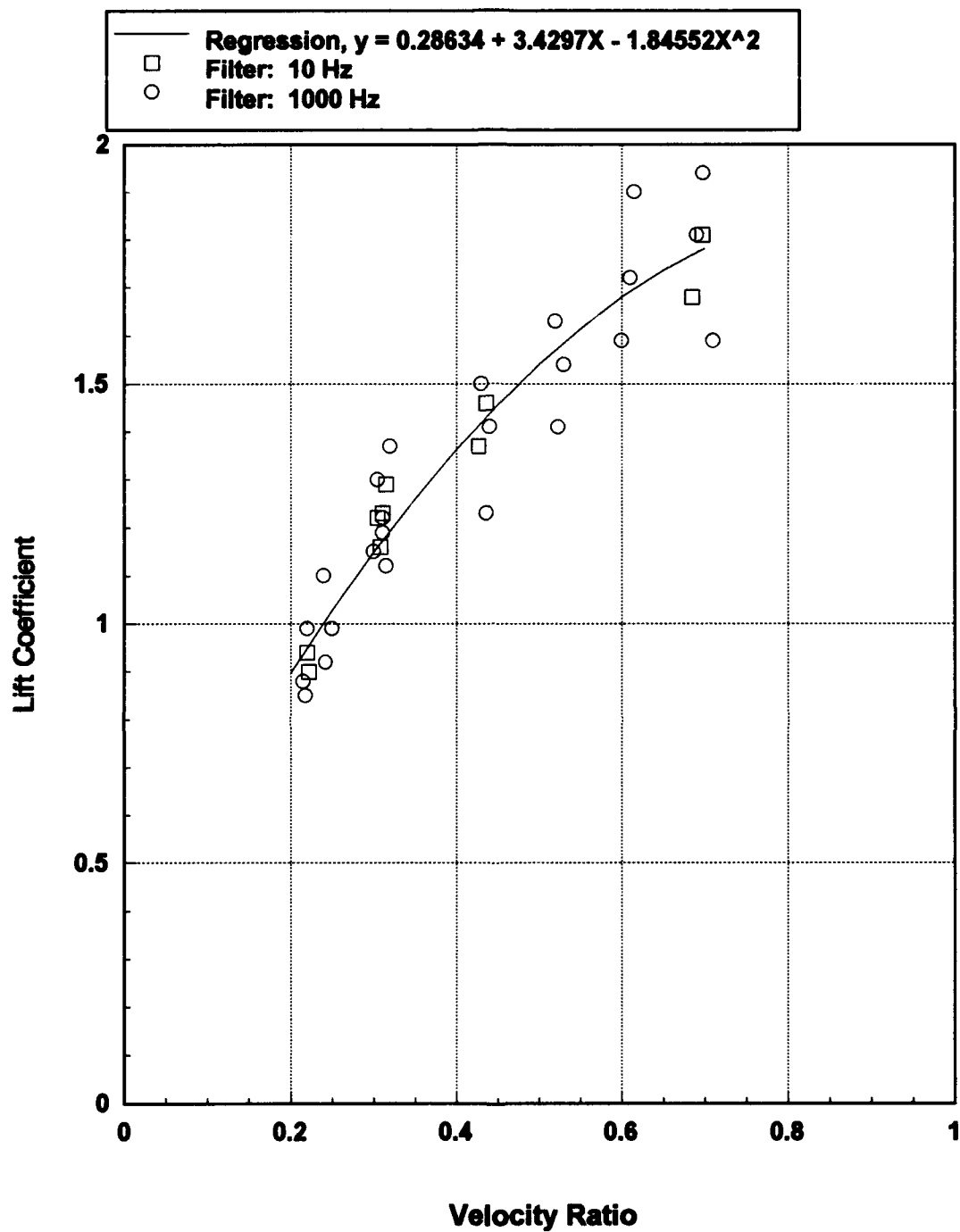


Figure 23. Lift Coefficient Versus Velocity Ratio for Same-RPM Tests in Primary Configuration

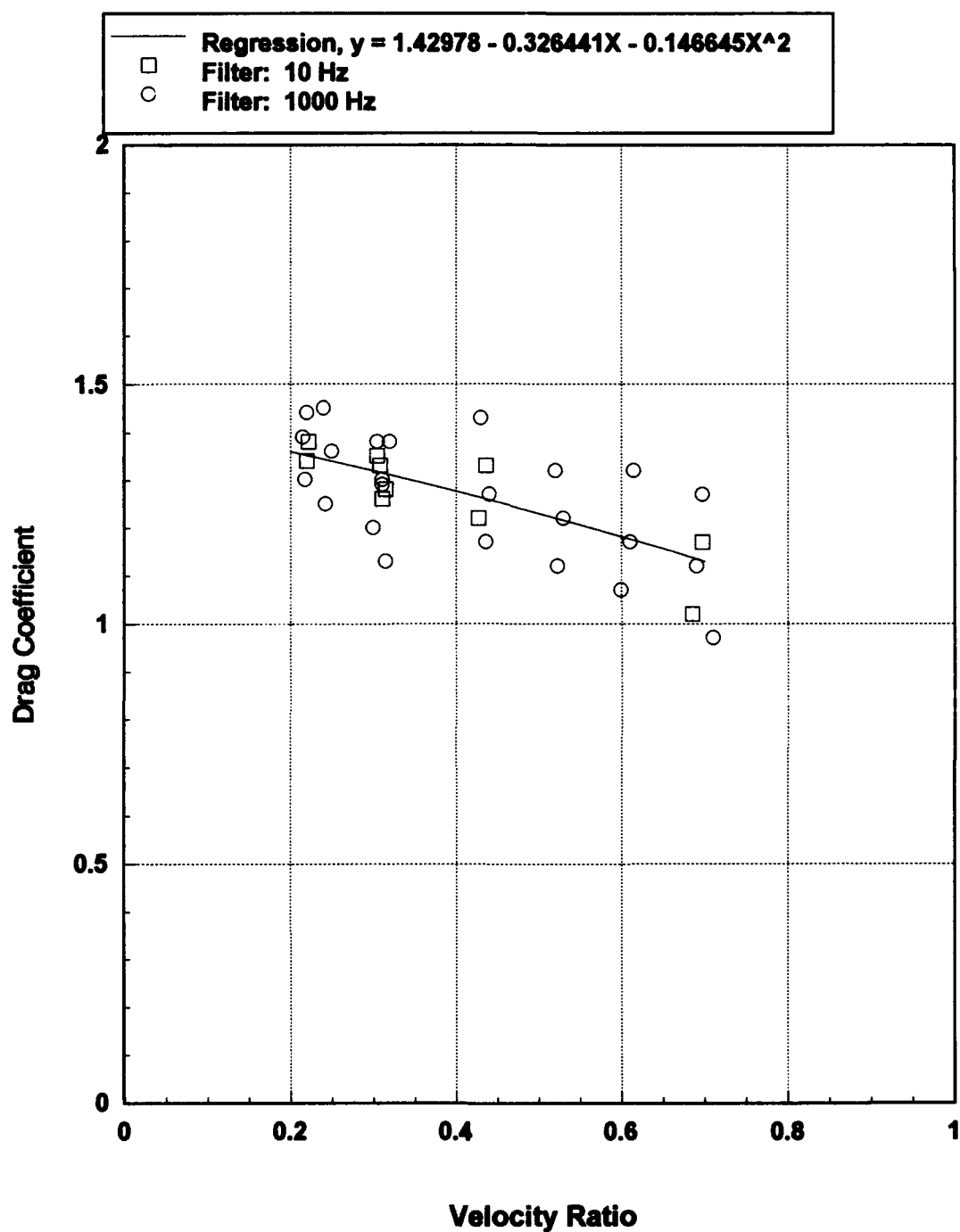


Figure 24. Drag Coefficient Versus Velocity Ratio for Same-RPM Tests in Primary Configuration

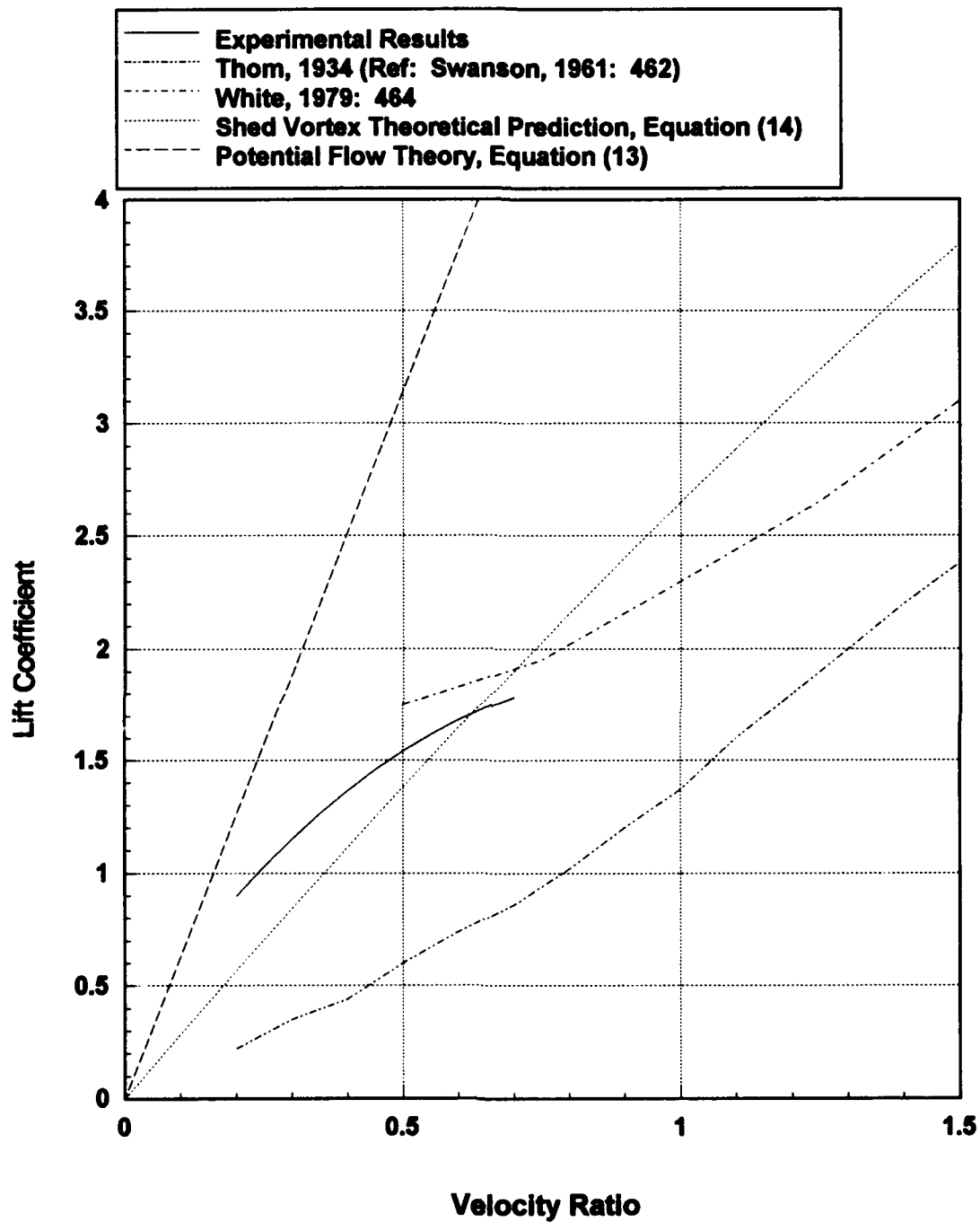


Figure 25. Comparison of Lift Coefficient Versus Velocity Ratio for Same-RPM Tests in Primary Configuration

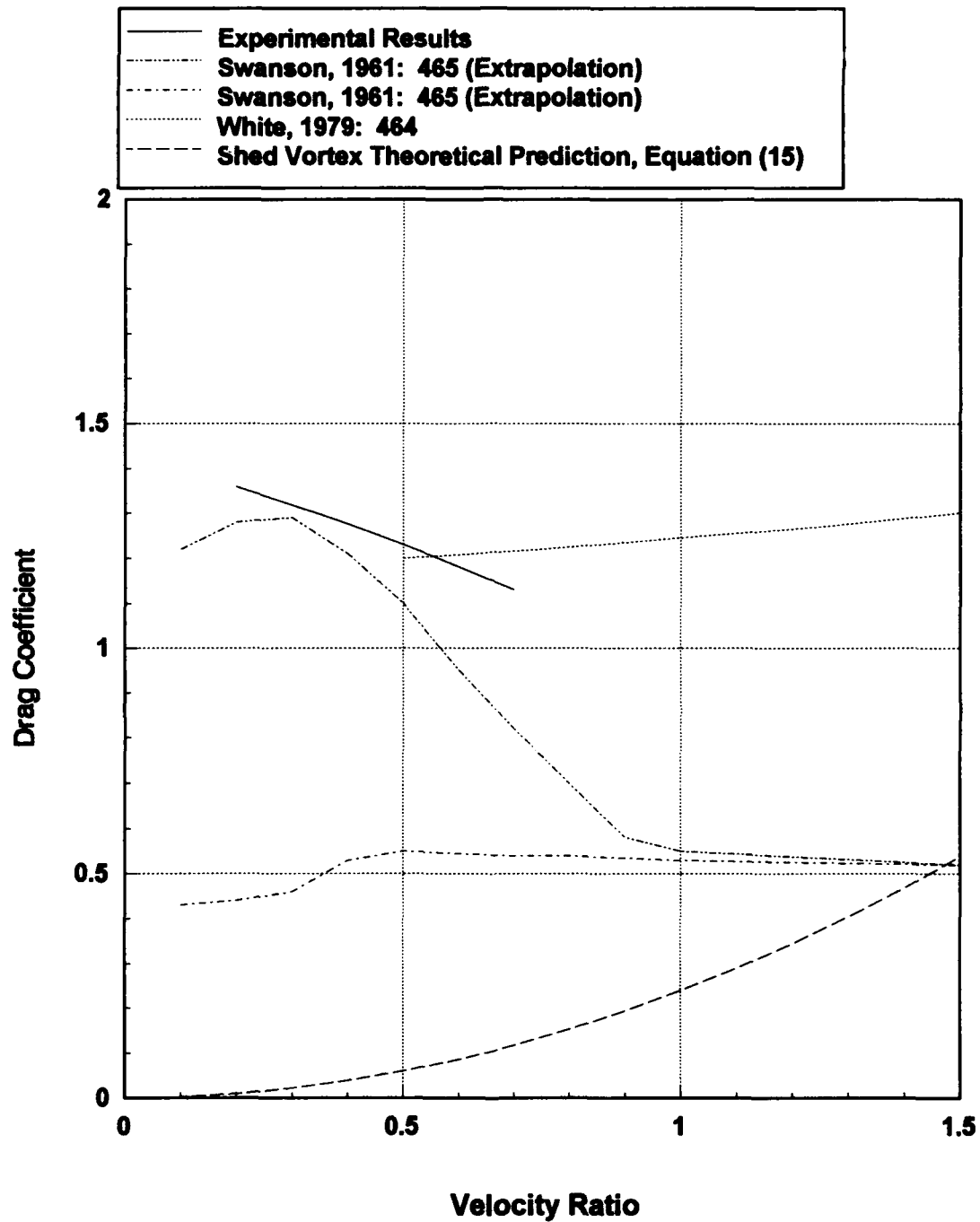


Figure 26. Comparison of Drag Coefficient Versus Velocity Ratio for Same-RPM Tests in Primary Configuration

Dual Cylinder Tests

With the single cylinder tests as a baseline, the angular speeds of the right cylinder were changed in 20% increments, both increasing and decreasing. The lift coefficient data for increasing and decreasing relative velocity ratios are shown in Figure 27. The results for drag coefficients from the same tests are presented in Figure 28. Here, both the increasing and decreasing relative velocity ratio tests are shown with only the most extreme case of $\pm 60\%$. This was done because the changes in drag coefficient are minimal, which was reasonable considering the fairly slight slope of the baseline drag data. Because of the small range of deviations, particularly relative to the level of uncertainty in the data (of up to about 7.5%), only inferences about the general trends were applicable. For the highest relative velocity ratios, the drag coefficients were slightly lower than for the lowest relative velocity ratio tests.

In the figures for both lift and drag, the maximum baseline velocity ratio is less for the varying velocity ratio tests than for the actual baseline tests. This is because the maximum angular speed tested was 8000 rpm for all these tests, and therefore the maximum baseline angular speed from which deviations were made was 5000 rpm. All the lift and drag coefficient data from these tests are listed in Appendix C in Table X.

The effects of one cylinder on the other during these tests with variant relative velocity ratios are shown in Figures 29 to 31. In these figures, the lines were determined by the single cylinder data regression only, by assuming no interactions took place between the two cylinders. The symbols represent what actually happened in the dual cylinder experiments, and indicate that assuming no interactions occurred between the cylinders would be reasonable, but becomes less accurate as the disparity between the two cylinders velocity ratios increases. These results are summarized in terms of percentages in Figure 31.

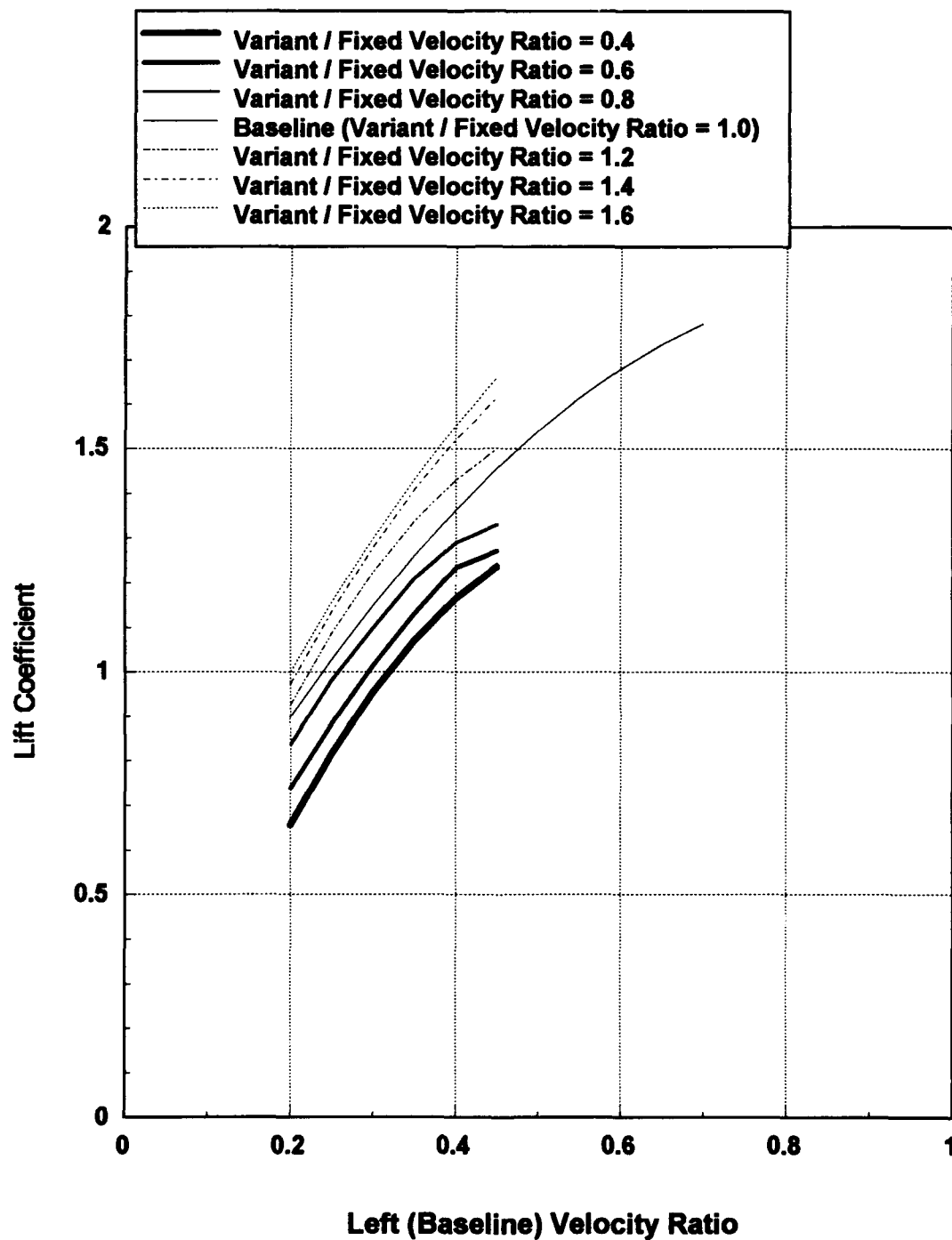


Figure 27. Lift Coefficient Data for Changing Relative Velocity Ratios

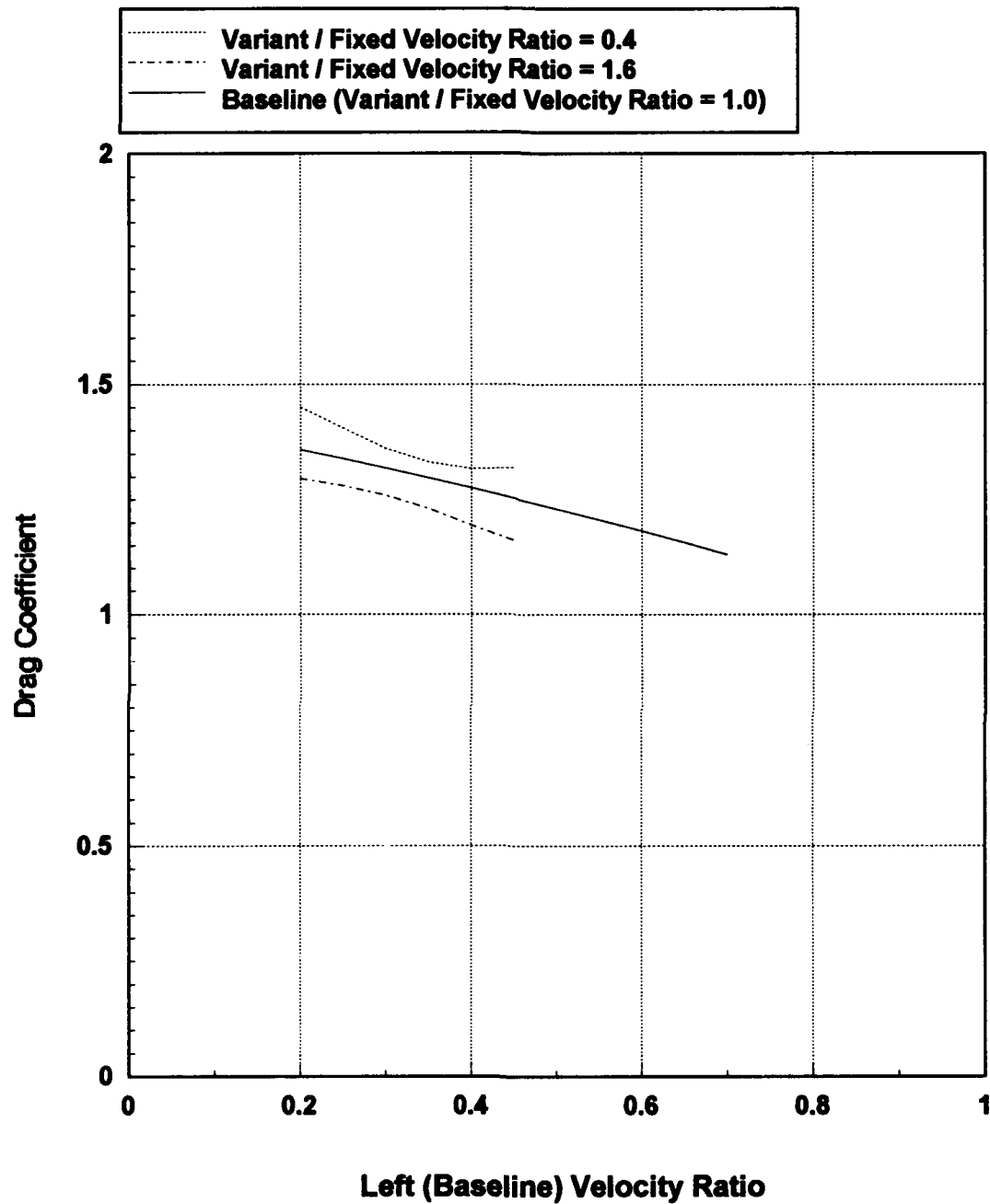


Figure 28. Drag Coefficient Data for Changing Relative Velocity Ratios

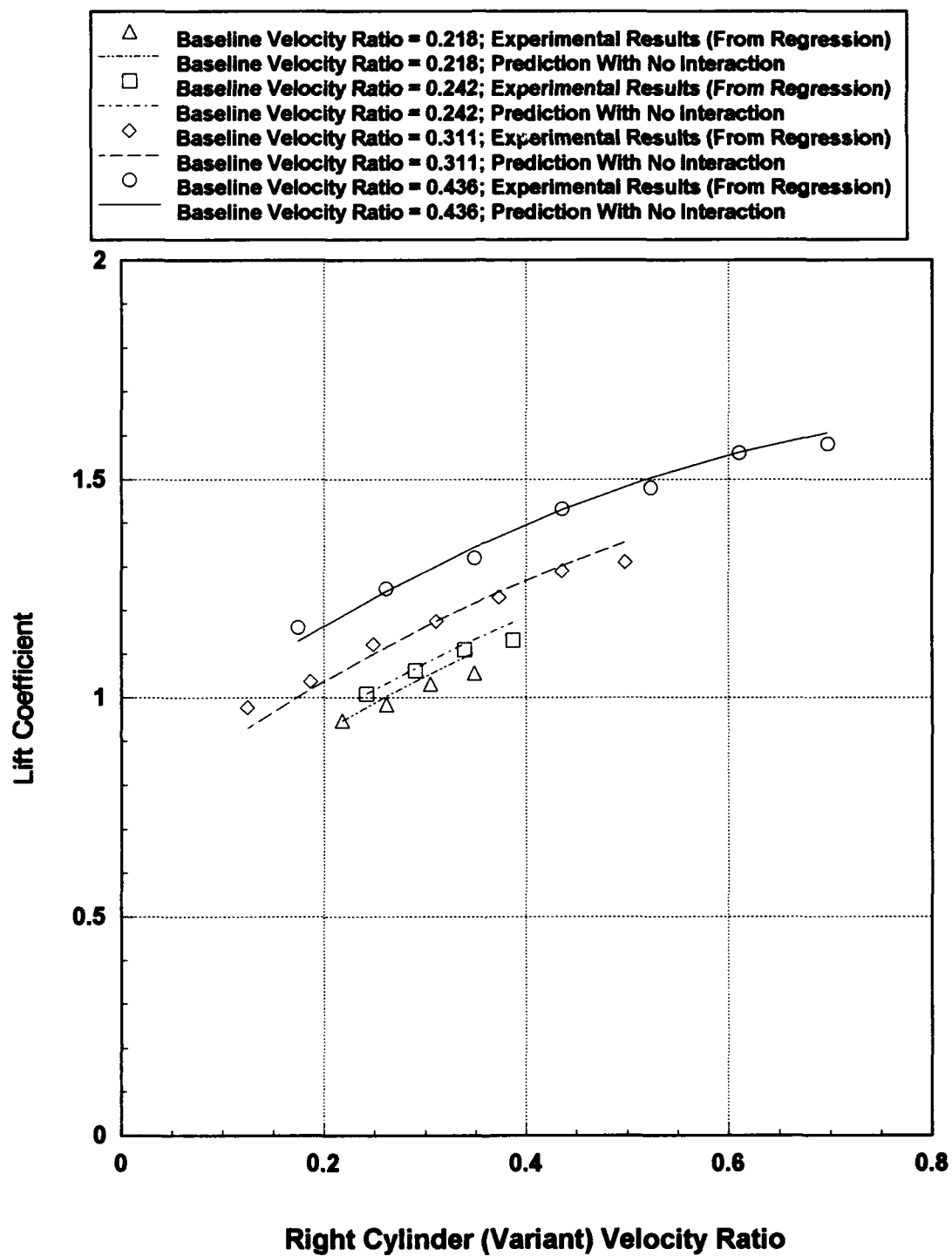


Figure 29. Variations in Lift Coefficient With Changing Relative Velocity Ratio

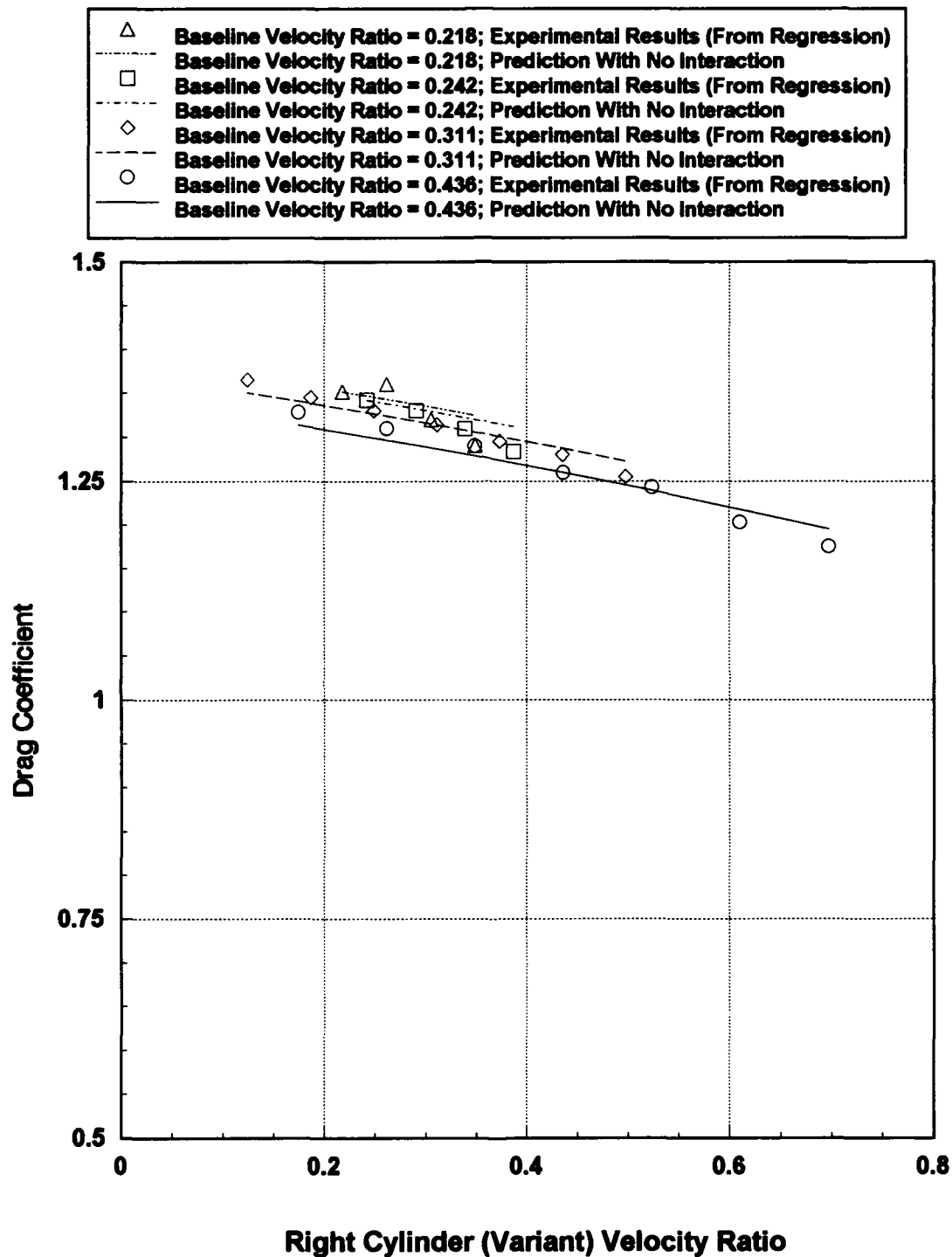


Figure 30. Variations in Drag Coefficient With Changing Relative Velocity Ratio

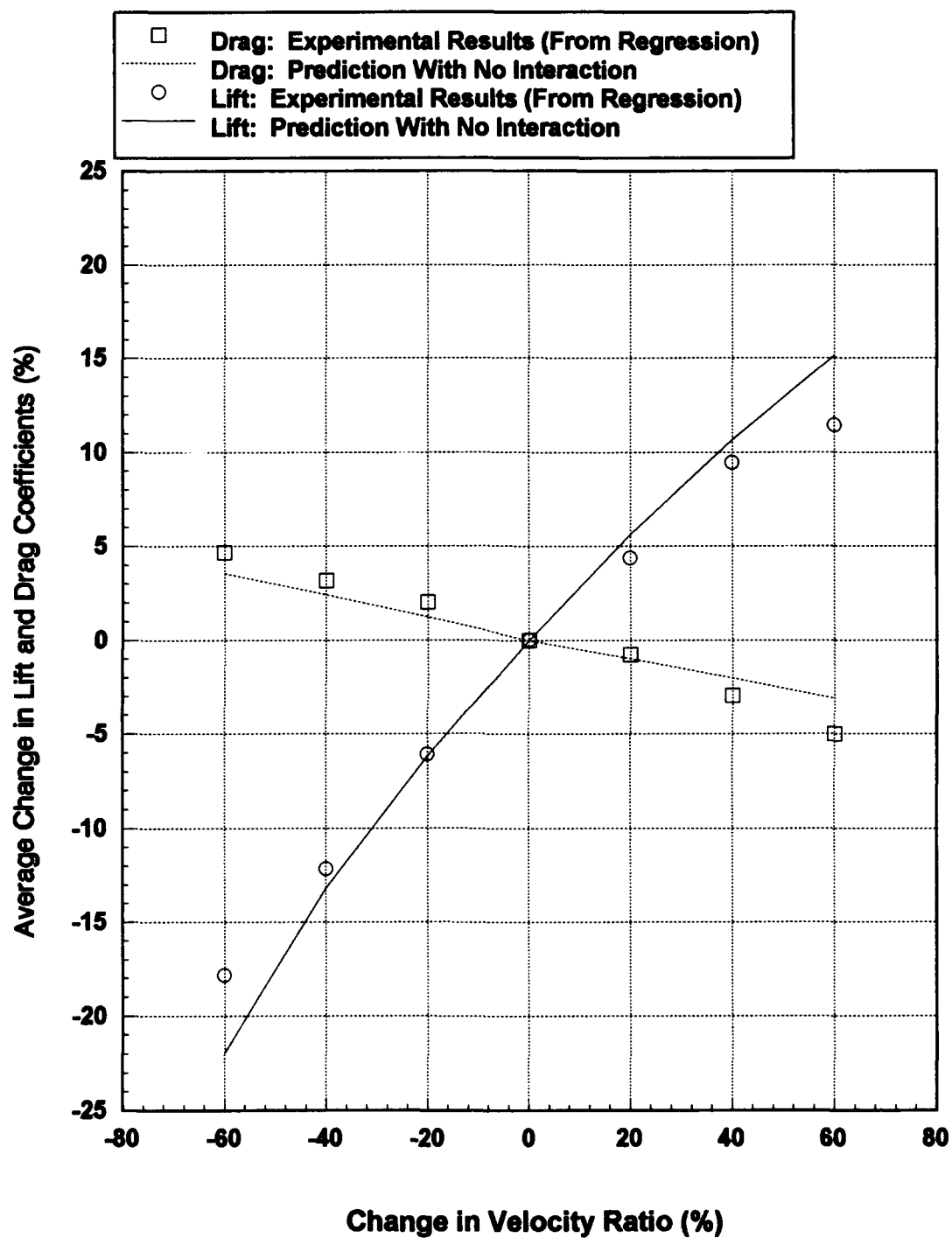


Figure 31. Percent Change in Lift and Drag Coefficients With Changing Relative Velocity Ratio

Offset Tests

Tests were also conducted with the two cylinders spinning at the same angular speeds in the secondary configuration, offset from direct crossflow by 30° . The purpose of these tests, like the drag coefficient versus Reynold's number tests previously described, was to determine if the normal component of velocity could be considered the only contributor to the forces on the cylinder, in this approximately two-dimensional configuration.

The results from these tests are in Figures 32 and 33. The data points from the offset tests are superimposed on the regressions from the primary configuration baseline results. To within the range of the data, over the velocity ratios tested and with the limited offset angle of 30° , treating the normal component of velocity as the sole contributor to the forces on the cylinders was seen to be valid. One noticable difference in these tests and those in the primary configuration was the angular speed at which the resonant vibrations which limited the maximum rotation rate set in. For these tests, that occurred at about 6000 rpm, as compared to 8000 rpm for the tests in the primary configuration. The reason for this was that the cylinders were spanning a longer distance inside the tunnel due to the 30° offset, so the support shaft allowed such vibrations at slower rotation rates. The data from these tests are also tabulated in Appendix C.

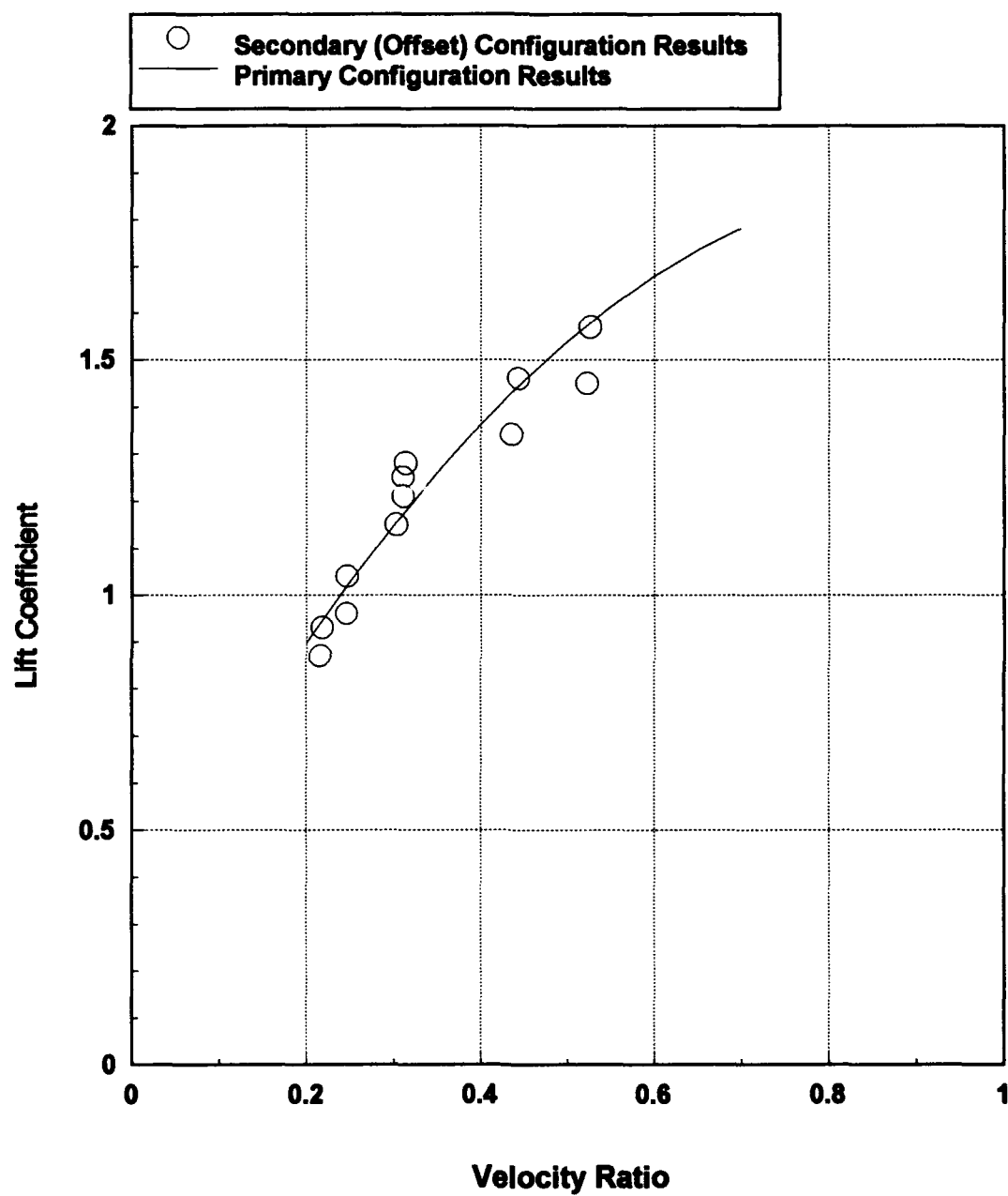


Figure 27. Lift Coefficient Versus Velocity Ratio for Secondary Configuration

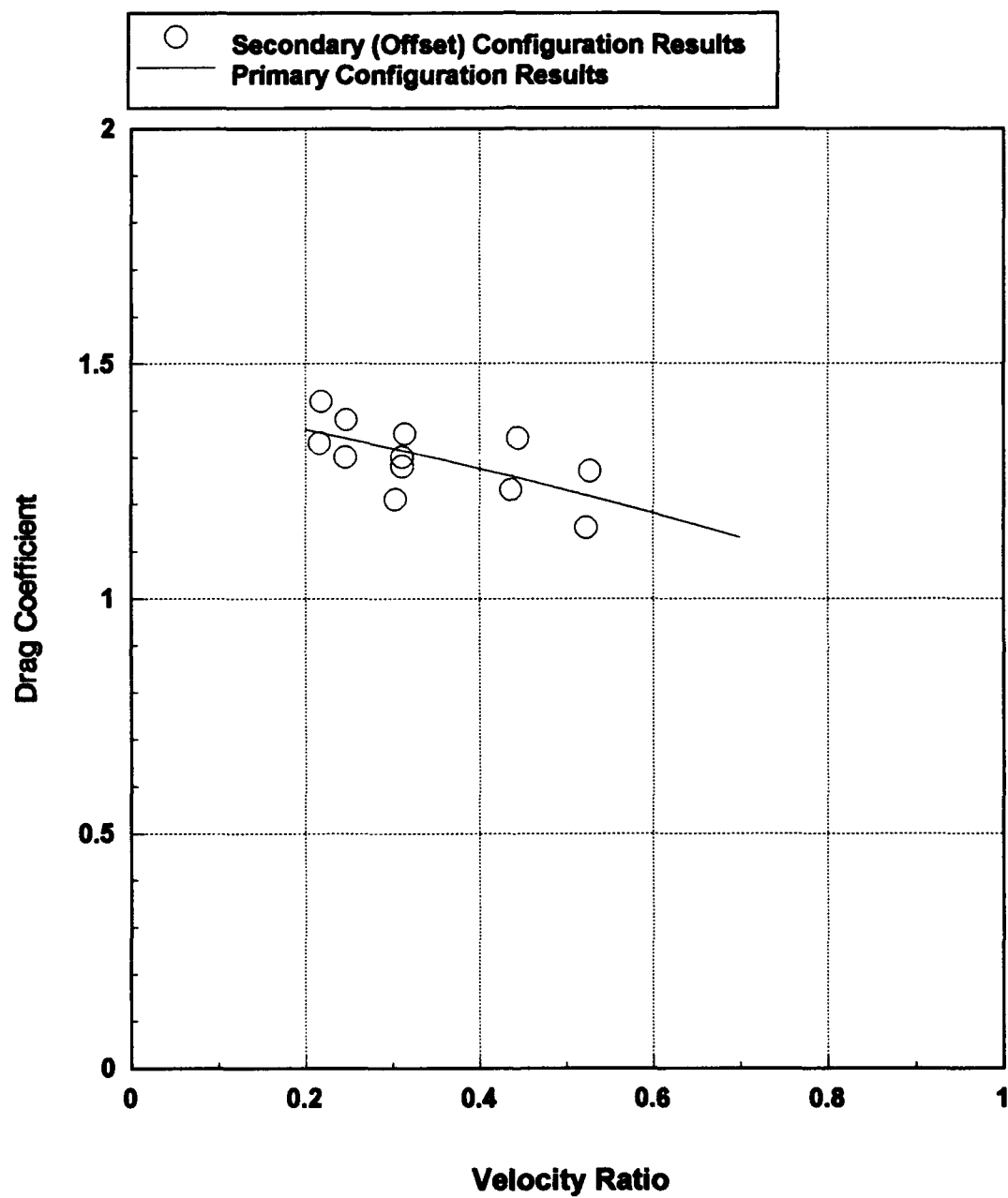


Figure 28. Drag Coefficient Versus Velocity Ratio for Secondary Configuration

Data Confidence and Possible Sources of Error

Several of the tests in this project were specifically designed to validate the ability of the experimental setup, with its strain gages on spoke rings and cylinders spanning beyond the width of the wind tunnel test section, to accurately measure forces. The static check loads to verify the calibrations, particularly those with a non-centered load, gave confidence in the ability of the setup to measure such loads accurately. The non-spinning tests to measure drag coefficients versus Reynolds number gave further confidence in the data, as these were actual aerodynamic forces being measured. The baseline spinning tests with both cylinders rotating together at the same angular rate were compared to some previous single cylinder results to give even further confidence in the data. The fact that previous results (Swanson, 1961: 462-464; White, 1979: 464) vary considerably in the range of velocity ratios tested (and beyond that range, in fact, previous data get even more disparate), could lead to skepticism about the magnitudes of forces measured in that region.

Such skepticism is important in experimentation, and even though attempts were made to validate the data presented in this report, and to generate high confidence in the data, it is prudent to examine and acknowledge possible sources of error. The most obvious potential source of error, and one which did in fact result in imperfect repeatability in the tests, was the slightly irregular rotation of the bearings within the spoke rings. Related to this could have been imperfect balance of the cylinders on their support shaft. Further, non-visible fluctuations and vibrations of the cylinders could have been in effect at low angular rates. Where vibrations became visible, tests were not conducted; in fact, it was believed that at higher angular rates the vibrations would continue to increase before subsiding, and would most probably cause the support shaft to shear and send the models down the wind tunnel. This, of course, was not validated by trial. Another possible source of error was variation in the angular rates and airspeed. These were set as

closely as possible to the target values, and the airspeed was far easier to set than was the rotation rate. Fortunately, the rotation rates were sampled along with the output from the strain gages, so even if the target was not reached exactly, the actual rotation rate at which the tests were conducted could be recorded. Finally, neglecting the interaction coefficients in the calibration of the strain gages could have introduced error. This was tested, however, and the check loads on the cylinders showed that any such errors were very small.

VI. Conclusions and Recommendations

Conclusions

Based on the results of the tests on independently rotating cylinders in this project, the following conclusions are made:

1. The experimental setup, with the cylinders extending beyond the width of the wind tunnel test section, and with strain gages mounted on spoke rings as load cells, is capable of measuring aerodynamic forces. Potential errors in the results from this setup are introduced by non-uniform rotation of the bearings within the spoke rings. These can be reduced by using a low frequency filter on the strain gage amplifiers.

2. The lift of independently rotating cylinders increases as one of the cylinders' velocity ratio is increased, but these elevations in lift diminish when the disparity between the two velocity ratios gets above about 40%. As the relative velocity ratio decreases, the lift also decreases. Changes in the drag on these cylinders with varying relative velocity ratios are within the range of uncertainty of these tests over the limited range of baseline velocity ratios tested.

3. Interactions between the two independently rotating cylinders increase as the disparity between the two cylinders' velocity ratios increases, over the range tested ($-60\% < \Delta\alpha < 60\%$). These interactions are slight below $\pm 40\%$ change in relative velocity ratio.

4. For an offset angle of 30° on an approximately two-dimensional cylinder test configuration, the normal component of freestream velocity may be treated as the only significant contributor to the forces on the cylinder.

Recommendations

• This project involved experimentation with a new and fairly unusual force measurement setup. Therefore, just as some questions about the aerodynamics of independently rotating cylinders were answered in a somewhat limited way, other questions were raised during the testing and analysis. For these reasons, the following recommendations are offered:

1. The range of velocity ratios tested in this project was limited by the rotation rate achievable with the cylinders powered by air-driven dental handpieces. Much more information could be obtained by reaching higher velocity ratios, but doing so will not be particularly easy. Several things might help in the effort to spin the cylinders faster. First, using a stronger support shaft should delay the onset of vibrations which made higher rotation rates unsafe. Second, having the assembly of cylinders, bearings, and support shaft professionally and dynamically balanced should make the cylinders rotate a little more smoothly, which would not only allow faster angular speeds, but might also reduce noise in the results. Finally, using air bearings, while it could be very tricky to measure forces, should provide both of these benefits as well. One thing to avoid in the effort to take the cylinders faster is using the wrong kind of drive mechanism. Other motors were tried for this project which were faster, but did not serve the ultimate purpose of collecting lift and drag data on the cylinders.

2. Besides covering a larger range of velocity ratios, another interesting aspect of independently rotating cylinders that was not addressed in this project involves looking at different kinds of data than actual forces on the cylinders. The aeronautics laboratory has just acquired equipment that could be used for sophisticated flow visualization and laser doppler anemometry. Using such equipment on the dual cylinder setup would provide much more insight into the aerodynamic phenomena at work, and should be considered.

Bibliography

- Anderson, John D. *Fundamentals of Aerodynamics*. New York: McGraw-Hill Book Company, 1984.
- Breuer, D. W. "The Fundamentals of Weapons Engineering," Volumes I and II, Air Force Institute of Technology, 1983.
- Badr, H. M., and S. C. R. Dennis. "Time-dependent Viscous Flow Past an Impulsively Started Rotating and Translating Circular Cylinder," *Journal of Fluid Mechanics*, 158: 447-488 (1985).
- Fornberg, Bengt. "Steady Viscous Flow Past a Circular Cylinder up to Reynolds Number 600," *Journal of Computational Physics*, 61: 297-320 (1985).
- Glauert, M. B. "A Boundary Layer Theorem, With Applications to Rotating Cylinders," *Journal of Fluid Mechanics*, 1: 89-99 (1956).
- Ingham, D. B., and T. Tang. "A Numerical Investigation into the Steady Flow Past a Rotating Circular Cylinder at Low and Intermediate Reynolds Numbers," *Journal of Computational Physics*, 87: 91-107 (1990).
- Jumper, George Y., C. J. Frushon, R. K. Longstreth, J. Smith, J. Willett, and D. Curtis, "Effect of Magnus Moments on Missile Aerodynamic Performance," Phillips Laboratory Technical Report (Draft Copy), September 9, 1991.
- Karamcheti, Krishnamurty. *Principles of Ideal-Fluid Aerodynamics*. New York: John Wiley and Sons, Inc. (1966).
- Kuethe, Arnold M., and Chuen-Yen Chow. *Foundations of Aerodynamics: Bases of Aerodynamic Design*. New York: John Wiley and Sons, Inc. (1986).
- Moore, D. W. "The Flow Past a Rapidly Rotating Circular Cylinder in a Uniform Stream," *Journal of Fluid Mechanics*, 2: 541-550 (1957).
- Reid, E. G. "Tests of Rotating Cylinders," NACA TN 209 (1924).

- Swanson, W. M. "The Magnus Effect: A Summary of Investigations to Date," *Journal of Basic Engineering*, 83: 461-470 (September 1961).
- Thom, A., "Experiments on the Air Forces on Rotating Cylinders," ARC R and M 1018 (1925).
- Thom, A., and S. R. Sengupta, "Air Torque on a Cylinder Rotating in an Air Stream," ARC R and M 1520 (1932).
- Thom, A., "Effects of Discs on the Air Forces on a Rotating Cylinder," ARC R and M 1623 (1934).
- White, Frank M. *Fluid Mechanics*. New York: McGraw-Hill Book Company, 1979.
- White, Frank M. *Viscous Fluid Flow*. New York: McGraw-Hill Book Company, 1991.
- Wood, W. W., "Boundary Layers Whose Streamlines are Closed," *Journal of Fluid Mechanics*, 1: 77-87 (1956).

Appendix A: Data Acquisition Program

The following BASIC program was used to collect data from the Pacific Instruments amplifiers, through the General Purpose Interface Bus (GPIB). The program also collected data from the frequency counters used to determine the angular speeds of the cylinders.

```
' Declarations for QuickBASIC 4.0/4.5 applications.

' NOTE : include this file only if you are using QuickBASIC Version 4.0
or
'         higher.

' Common GPIB status variables

COMMON SHARED /NISTATBLK/ ibsta%, iberr%, IBCNT%

' GPIB Subroutine Declarations

DECLARE SUB IBBNA (BD%, BDNAME$)
DECLARE SUB IBCAC (BD%, V%)
DECLARE SUB IBCLR (BD%)
DECLARE SUB IBCMD (BD%, CMD$)
DECLARE SUB IBCMDA (BD%, CMD$)
DECLARE SUB IBDMA (BD%, V%)
DECLARE SUB IBEOS (BD%, V%)
DECLARE SUB IBEOT (BD%, V%)
DECLARE SUB IBFIND (BDNAME$, BD%)
DECLARE SUB IBGTS (BD%, V%)
DECLARE SUB IBIST (BD%, V%)
DECLARE SUB IBLOC (BD%)
DECLARE SUB IBONL (BD%, V%)
DECLARE SUB IBPAD (BD%, V%)
DECLARE SUB IBPCT (BD%)
DECLARE SUB IBPPC (BD%, V%)
DECLARE SUB IBRD (BD%, RD$)
DECLARE SUB IBRDA (BD%, RD$)
DECLARE SUB IBRDF (BD%, FLNAME$)
DECLARE SUB IBRDI (BD%, IARR%(), CNT%)
DECLARE SUB IBRDIA (BD%, IARR%(), CNT%)
DECLARE SUB IBRPP (BD%, PPR%)
DECLARE SUB IBRSC (BD%, V%)
DECLARE SUB IBRSP (BD%, SPR%)
DECLARE SUB IBRSV (BD%, V%)
DECLARE SUB IBSAD (BD%, V%)
DECLARE SUB IBSIC (BD%)
DECLARE SUB IBSRE (BD%, V%)
```

```

DECLARE SUB IBSTOP (BD%)
DECLARE SUB IBTMO (BD%, V%)
DECLARE SUB IBTRAP (MASK%, MODE%)
DECLARE SUB IBTRG (BD%)
DECLARE SUB IBWAIT (BD%, MASK%)
DECLARE SUB IBWRT (BD%, WRT$)
DECLARE SUB IBWRTA (BD%, WRT$)
DECLARE SUB IBWRTF (BD%, FLNAME$)
DECLARE SUB IBWRTI (BD%, IARR%(), CNT%)
DECLARE SUB IBWRTIA (BD%, IARR%(), CNT%)

```

' GPIB Function Declarations

```

DECLARE FUNCTION ILBNA% (BD%, BDNAMES$)
DECLARE FUNCTION ILCAC% (BD%, V%)
DECLARE FUNCTION ILCLR% (BD%)
DECLARE FUNCTION ILCMD% (BD%, CMD$, CNT%)
DECLARE FUNCTION ILCMDA% (BD%, CMD$, CNT%)
DECLARE FUNCTION ILDMA% (BD%, V%)
DECLARE FUNCTION ILEOS% (BD%, V%)
DECLARE FUNCTION ILEOT% (BD%, V%)
DECLARE FUNCTION ILFIND% (BDNAMES$)
DECLARE FUNCTION ILGTS% (BD%, V%)
DECLARE FUNCTION ILIST% (BD%, V%)
DECLARE FUNCTION ILLOC% (BD%)
DECLARE FUNCTION ILONL% (BD%, V%)
DECLARE FUNCTION ILPAD% (BD%, V%)
DECLARE FUNCTION ILPCT% (BD%)
DECLARE FUNCTION ILPPC% (BD%, V%)
DECLARE FUNCTION ILRD% (BD%, RD$, CNT%)
DECLARE FUNCTION ILRDA% (BD%, RD$, CNT%)
DECLARE FUNCTION ILRDF% (BD%, FLNAME$)
DECLARE FUNCTION ILRDI% (BD%, IARR%(), CNT%)
DECLARE FUNCTION ILRDIA% (BD%, IARR%(), CNT%)
DECLARE FUNCTION ILRPP% (BD%, PPR%)
DECLARE FUNCTION ILRSC% (BD%, V%)
DECLARE FUNCTION ILRSP% (BD%, SPR%)
DECLARE FUNCTION ILRSV% (BD%, V%)
DECLARE FUNCTION ILSAD% (BD%, V%)
DECLARE FUNCTION ILSIC% (BD%)
DECLARE FUNCTION ILSRE% (BD%, V%)
DECLARE FUNCTION ILSTOP% (BD%)
DECLARE FUNCTION ILTMO% (BD%, V%)
DECLARE FUNCTION ILTRAP% (MASK%, MODE%)
DECLARE FUNCTION ILTRG% (BD%)
DECLARE FUNCTION ILWAIT% (BD%, MASK%)
DECLARE FUNCTION ILWRT% (BD%, WRT$, CNT%)
DECLARE FUNCTION ILWRTA% (BD%, WRT$, CNT%)
DECLARE FUNCTION ILWRTF% (BD%, FLNAME$)
DECLARE FUNCTION ILWRTI% (BD%, IARR%(), CNT%)
DECLARE FUNCTION ILWRTIA% (BD%, IARR%(), CNT%)
CLS

```

```

COLOR , 1
KEY(1) ON
KEY(2) ON
KEY(3) ON
KEY(4) ON
KEY(5) ON
KEY(10) ON

LP:
COLOR , 1
LOCATE 3, 1
PRINT "F1- USER INPUT FOR DATA FILE"
PRINT
PRINT "F2- VIEW CHANNEL VOLTAGES"
PRINT
PRINT "F3- VIEW RPM"
PRINT
PRINT "F4- ZERO THE AMPLIFIERS"
PRINT
PRINT "F5- ACQUIRE RPM AND CHANNEL VOLTAGES"
PRINT
PRINT "F10- END"
ON KEY(1) GOSUB FILEE:
ON KEY(2) GOSUB PACAMP:
ON KEY(3) GOSUB RPM:
ON KEY(4) GOSUB ZERRO:
ON KEY(5) GOSUB DATAAQ:
ON KEY(10) GOSUB EEE:

GOTO LP:

EEE:
CLOSE
END

FILEE:
CLOSE
COLOR , 0
CLS
COLOR , 1
INPUT "NAME DATA FILE FOR DATA STORAGE:   XXXXX NO EXTENSION   "; NA$
COLOR , 0
CLS
COLOR , 1
NA$ = "C:\DATA\" + NA$ + ".DAT"
OPEN NA$ FOR OUTPUT AS #1                                'DATA FILE
RETURN
PACAMP:
COLOR , 0

```

```

CLS
COLOR , 1
UDNAME$ = "DEV2"
BOARD
CALL IBFIND(UDNAME$, DEV2%)

LOCATE 1, 15
PRINT "CH1"
LOCATE 1, 30
PRINT "CH2"
LOCATE 1, 45
PRINT "CH3"
LOCATE 1, 60
PRINT "CH4"
CHANV:

      chnn$(1) = "s1"
      chnn$(2) = "s2"
      chnn$(3) = "s3"
      chnn$(4) = "s4"

      chloc = 15
      FOR ch = 1 TO 4
        volt1 = 0
        volt = 0

        WRT$ = chnn$(ch) + CHR$(&HA)
        CALL IBWRT(DEV2%, WRT$)

      FOR I = 1 TO 11
        WRT$ = "rld1" + CHR$(&HA)
        CALL IBWRT(DEV2%, WRT$)

      RD$ = SPACE$(2)
      CALL IBRD(DEV2%, RD$)

      A$ = MID$(RD$, 1)
      B$ = MID$(RD$, 2)
      IF (ASC(B$) AND 240) = 240 THEN
        c = (((ASC(B$)) AND 15) * 256 + ASC(A$)) - 4096
      ELSE
        c = ((ASC(B$)) AND 15) * 256 + ASC(A$)
      END IF
      volt = c * .0048828
      volt1 = volt1 + volt

      NEXT I
      ' CALL IBCLR(DEV2%)

```

```

        LOCATE 3, chloc
        PRINT USING "##.###"; (volt1 / 11);
        chloc = chloc + 15
    NEXT ch
    DD$ = INKEY$

    IF (VAL(DD$)) > 0 THEN
        GOTO FFF:
    ELSE

        GOTO CHANV:
    END IF

FFF:
    COLOR , 0
    CLS 2
    RETURN

RPM:
    COLOR , 0
    CLS 2
    COLOR , 1
RPMDA:
    UDNAME$ = "DEV14"                                'GPIB
    BOARD

    CALL IBFIND(UDNAME$, DEV14%)
    WRT$ = "FNC SQW FREQ :CH00 SRX FREQ 10 SRN FREQ 100 SET VOLT 2
    SET TRLV 1.5 SET BAND 10000" + CHR$(&HD) + CHR$(&HA)
    CALL IBWRT(DEV14%, WRT$)

    CALL IBCLR(DEV14%)
    WRT$ = "INX FREQ" + CHR$(&HD) + CHR$(&HA)
    CALL IBWRT(DEV14%, WRT$)

    WRT$ = "FTH FREQ" + CHR$(&HD) + CHR$(&HA)
    CALL IBWRT(DEV14%, WRT$)

    FOR I = 1 TO 70000
    NEXT I
    RD$ = SPACE$(40)
    CALL IBRD(DEV14%, RD$)

    A! = VAL(RD$) * 60
    LOCATE 3, 10
    PRINT USING "#####"; A!
    'CALL IBCLR(DEV14%)

    UDNAME$ = "DEV15"                                'GPIB
    BOARD

```

```

CALL IBFIND(UDNAME$, DEV15%)
WRT$ = "FNC SQW FREQ :CH00 SRX FREQ 10 SRN FREQ 100 SET VOLT 2
SET TRLV 1.5 SET BAND 10000" + CHR$(&HD) + CHR$(&HA)
CALL IBWRT(DEV15%, WRT$)

CALL IBCLR(DEV15%)
WRT$ = "INX FREQ" + CHR$(&HD) + CHR$(&HA)
CALL IBWRT(DEV15%, WRT$)

WRT$ = "FTH FREQ" + CHR$(&HD) + CHR$(&HA)
CALL IBWRT(DEV15%, WRT$)

FOR I = 1 TO 70000
NEXT I
RD$ = SPACE$(40)
CALL IBRD(DEV15%, RD$)
B! = VAL(RD$) * 60
LOCATE 3, 20
PRINT USING "#####"; B!

'CALL IBCLR(DEV15%)

DD$ = INKEY$

IF (VAL(DD$)) > 0 THEN
GOTO RRR:
ELSE

GOTO RPYMDA:
END IF

RRR:
COLOR , 0
CLS 2
RETURN

ZERRO:

COLOR , 0
CLS
COLOR , 1
UDNAME$ = "DEV2"
BOARD
CALL IBFIND(UDNAME$, DEV2%)

WRT$ = "s1n4" + CHR$(&HA)
CALL IBWRT(DEV2%, WRT$)
WRT$ = "b1" + CHR$(&HA)

```

'GPIB

```

CALL IBWRT(DEV2%, WRT$)
WRT$ = "1DONE" + CHR$(&HA)
CALL IBWRT(DEV2%, WRT$)

RETURN

DATAAQ:

COLOR , 0
CLS 2
COLOR , 1
LOCATE 1, 15
PRINT "RPM1"
LOCATE 1, 25
PRINT "RPM2"
DDDD:
UDNAME$ = "DEV14"                                'GPIB
BOARD

CALL IBFIND(UDNAME$, DEV14%)
WRT$ = "FNC SQW FREQ :CH00 SRX FREQ 10 SRN FREQ 100 SET VOLT 2
SET TRLV 1.5 SET BAND 10000" + CHR$(&HD) + CHR$(&HA)
CALL IBWRT(DEV14%, WRT$)

CALL IBCLR(DEV14%)

WRT$ = "INX FREQ" + CHR$(&HD) + CHR$(&HA)
CALL IBWRT(DEV14%, WRT$)

WRT$ = "FTH FREQ" + CHR$(&HD) + CHR$(&HA)
CALL IBWRT(DEV14%, WRT$)

FOR I = 1 TO 70000
NEXT I
RD$ = SPACE$(40)
CALL IBRD(DEV14%, RD$)
A! = VAL(RD$) * 60
LOCATE 3, 15
PRINT #1, USING "##### "; A!;
PRINT USING "#####"; A!

UDNAME$ = "DEV15"                                'GPIB
BOARD

CALL IBFIND(UDNAME$, DEV15%)
WRT$ = "FNC SQW FREQ :CH00 SRX FREQ 10 SRN FREQ 100 SET VOLT 2
SET TRLV 1.5 SET BAND 10000" + CHR$(&HD) + CHR$(&HA)
CALL IBWRT(DEV15%, WRT$)

```

```

        CALL IBCLR(DEV15%)
        WRT$ = "INX FREQ" + CHR$(&HD) + CHR$(&HA)
        CALL IBWRT(DEV15%, WRT$)

        WRT$ = "FTH FREQ" + CHR$(&HD) + CHR$(&HA)
        CALL IBWRT(DEV15%, WRT$)

FOR I = 1 TO 70000
NEXT I
    RD$ = SPACE$(40)
    CALL IBRD(DEV15%, RD$)
    B! = VAL(RD$) * 60
    LOCATE 3, 25
    PRINT #1, USING "##### "; B!;
    PRINT USING "#####"; B!

COLOR , 1
UDNAME$ = "DEV2"
BOARD
    CALL IBFIND(UDNAME$, DEV2%)

    LOCATE 1, 35
    PRINT "CH1"
    LOCATE 1, 45
    PRINT "CH2"
    LOCATE 1, 55
    PRINT "CH3"
    LOCATE 1, 65
    PRINT "CH4"

    chnn$(1) = "s1"
    chnn$(2) = "s2"
    chnn$(3) = "s3"
    chnn$(4) = "s4"

    chloc = 35
    FOR ch = 1 TO 4
    volt1 = 0
    volt = 0

        WRT$ = chnn$(ch) + CHR$(&HA)
        CALL IBWRT(DEV2%, WRT$)

    FOR I = 1 TO 11
        WRT$ = "r1d1" + CHR$(&HA)
        CALL IBWRT(DEV2%, WRT$)

```

```

RD$ = SPACE$(2)
CALL IBRD(DEV2%, RD$)

A$ = MID$(RD$, 1)
B$ = MID$(RD$, 2)
IF (ASC(B$) AND 240) = 240 THEN
c = (((ASC(B$)) AND 15) * 256 + ASC(A$)) - 4096
ELSE
c = ((ASC(B$)) AND 15) * 256 + ASC(A$)
END IF
volt = c * .0048828
volt1 = volt1 + volt

NEXT I
' CALL IBCLR(DEV2%)
LOCATE 3, chloc
PRINT #1, USING "##.### "; (volt1 / 11);
PRINT USING "##.###"; (volt1 / 11);
chloc = chloc + 10
NEXT ch
DD$ = INKEY$

IF (VAL(DD$)) > 0 THEN
GOTO GGG:
ELSE
PRINT #1,
GOTO DDDD:
END IF

GGG:
COLOR , 0
CLS 2
CLS
RETURN

```

Appendix B: Data Reduction Example

As an example of the data reduction process for the spinning cylinder tests, one of the baseline points is included here in detail.

Test Conditions: $T = 292 \text{ K}$

$$p = 28.95 \text{ inches Hg} = 98020 \text{ N/m}^2$$

$$\rho = 1.17 \text{ kg/m}^3$$

$$V_{\infty} = 100 \text{ ft/s} = 30.48 \text{ m/s}$$

Rotation rate = 4930 RPM

$$\omega_0 = \frac{2\pi}{60}(4930) = 516.3 \text{ radians/sec}$$

$$\text{Velocity Ratio: } \alpha = \frac{\omega_0 R}{V_{\infty}} = \frac{(516.3 / \text{sec})(0.0417 \text{ ft})}{100 \text{ ft / sec}} = 0.215$$

Magnitude of outputs from strain gages (mV):

Left Vertical: 50

Left Horizontal: 57

Right Vertical: 36

Right Horizontal: 56

Application of calibrations to get forces (N):

$$\text{Left Vertical: } F = \frac{50 - 3.995578}{24.4343} = 1.88$$

$$\text{Left Horizontal: } F = \frac{57 - 0.35034}{19.3045} = 2.93$$

$$\text{Right Vertical: } F = \frac{36 - 2.09184}{18.6658} = 1.82$$

$$\text{Right Horizontal: } F = \frac{56 - 3.76871}{17.8676} = 2.92$$

$$\text{Lift} = 3.70 \text{ N}$$

$$\text{Drag} = 5.85 \text{ N}$$

$$c_l = \frac{\text{Lift}}{\frac{1}{2} \rho V_{\infty}^2 (\text{Diameter})(\text{Length})}$$

$$c_l = \frac{3.70 \text{ kg m/s}^2}{\left(\frac{1}{2}\right) \left(1.17 \text{ kg/m}^3\right) \left(30.48 \text{ m/s}\right)^2 (0.0254 \text{ m})(0.3048 \text{ m})}$$

$$c_l = 0.88$$

$$c_d = \frac{\textit{Drag}}{\frac{1}{2}\rho V_\infty^2 (\textit{Diameter})(\textit{Length})}$$

$$c_d = 1.39$$

This process was automated to some extent by a FORTRAN computer program.

Appendix C: Experimental Data

This appendix contains the tabulated results from the experiments, as referenced in the *Results* chapter.

TABLE IV.
Calibrations of Primary Configuration.

Weight on Load Cell (Horizontal or Vertical, kg)	Force on Load Cell (Horizontal or Vertical, N)	Left Vertical Bridge Output (mV)	Right Vertical Bridge Output (mV)	Left Horizontal Bridge Output (mV)	Right Horizontal Bridge Output (mV)
0.05	0.49	14	10	-8	12
0.05	0.49	15	11	-9	13
0.05	0.49	16	13	-11	14
0.1	0.98	26	20	-19	19
0.1	0.98	28	22	-20	20
0.1	0.98	28	23	-20	22
0.25	2.45	62	47	-47	46
0.25	2.45	64	49	-48	48
0.25	2.45	65	50	-50	48
0.5	4.9	121	92	-94	90
0.5	4.9	123	94	-95	91
0.5	4.9	124	95	-97	93

TABLE V.
Calibrations of Secondary Configuration.

Weight on Load Cell (Horizontal or Vertical, kg)	Force on Load Cell (Horizontal or Vertical, N)	Left Vertical Bridge Output (mV)	Right Vertical Bridge Output (mV)	Left Horizontal Bridge Output (mV)	Right Horizontal Bridge Output (mV)
0.05	0.49	7	9	15	8
0.05	0.49	9	9	16	8
0.05	0.49	9	10	17	9
0.1	0.98	17	18	35	18
0.1	0.98	17	19	35	19
0.1	0.98	19	19	36	19
0.25	2.45	47	48	87	47
0.25	2.45	48	48	88	48
0.25	2.45	49	49	89	48
0.5	4.9	99	96	180	93
0.5	4.9	99	97	182	94
0.5	4.9	100	99	184	95

TABLE VI.
Drag Coefficient Versus Reynold's Number Tests for Primary Configuration.

Freestream Velocity (ft/s)	Freestream Velocity (m/s)	Reynold's Number	Drag Coefficient
50	15.24	24978	1.33
50	15.24	24978	1.39
60	18.29	29977	1.35
60	18.29	29977	1.38
70	21.34	34976	1.27
70	21.34	34976	1.30
80	24.38	39959	1.23
80	24.38	39959	1.21
90	27.43	44958	1.14
90	27.43	44958	1.12
100	30.48	49957	1.10
100	30.48	49957	1.09

TABLE VII.
Drag Coefficient Versus Reynold's Number Tests for Secondary Configuration.

Tunnel Velocity (ft/s)	Normal Velocity (ft/s)	Normal Velocity (m/s)	Reynold's Number	Drag Coefficient
57.73	50	15.24	24628	1.30
57.73	50	15.24	24628	1.35
69.28	60	18.29	29553	1.31
69.28	60	18.29	29553	1.34
80.83	70	21.34	34479	1.26
80.83	70	21.34	34479	1.30
92.38	80	24.38	39405	1.22
92.38	80	24.38	39405	1.25
103.9	90	27.43	44330	1.18
103.9	90	27.43	44330	1.20
115.5	100	30.48	49256	1.15
115.5	100	30.48	49256	1.18

TABLE VIII.
Single-Cylinder Tests Results for Primary Configuration, Filter of 1kHz.

Freestream Velocity (ft/s)	Left and Right RPM	Left and Right Velocity Ratio	Lift Coefficient	Drag Coefficient
100	4930	0.215	0.88	1.39
100	5000	0.218	0.85	1.30
100	5045	0.220	0.99	1.44
90	4950	0.241	1.10	1.45
90	5000	0.242	0.92	1.25
90	5160	0.250	0.99	1.36
70	4820	0.301	1.15	1.20
70	4900	0.305	1.30	1.38
70	5000	0.311	1.22	1.30
56	4000	0.311	1.19	1.29
56	4045	0.315	1.12	1.13
56	4110	0.320	1.37	1.38
50	4930	0.430	1.50	1.43
50	5000	0.436	1.23	1.17
50	5045	0.440	1.41	1.27
50	5960	0.520	1.63	1.32
50	6000	0.523	1.41	1.12
50	6080	0.529	1.54	1.22
50	6880	0.600	1.59	1.07
50	7000	0.610	1.72	1.17
50	7050	0.615	1.90	1.32
50	7910	0.690	1.81	1.12
50	8000	0.698	1.94	1.27
50	8140	0.710	1.59	0.97

TABLE IX.
Single-Cylinder Tests Results for Primary Configuration, Filter of 10 Hz.

Freestream Velocity (ft/s)	Left and Right RPM	Left and Right Velocity Ratio	Lift Coefficient	Drag Coefficient
100	5050	0.220	0.90	1.38
100	5100	0.222	0.94	1.34
70	4900	0.305	1.22	1.35
70	5050	0.315	1.29	1.28
56	4000	0.311	1.23	1.26
56	3950	0.308	1.16	1.33
50	5000	0.436	1.46	1.33
50	4900	0.427	1.37	1.22
50	8000	0.697	1.81	1.17
50	7850	0.685	1.68	1.02

TABLE X.
Dual-Cylinder Tests Results for Primary Configuration.

Left (Fixed) Cylinder Velocity Ratio	Right (Variant) Cylinder Velocity Ratio	Percent Difference in Velocity Ratios	Lift Coefficient	Drag Coefficient
0.215	0.262	21.9	0.98	1.36
0.218	0.259	18.8	0.95	1.28
0.220	0.264	20.0	1.03	1.45
0.241	0.289	19.9	1.12	1.41
0.242	0.291	20.2	1.02	1.24
0.250	0.293	17.2	1.06	1.32
0.301	0.373	23.9	1.20	1.19
0.305	0.374	22.6	1.33	1.36
0.311	0.376	20.9	1.24	1.28
0.311	0.372	19.6	1.23	1.26
0.315	0.374	18.7	1.16	1.12
0.320	0.377	17.8	1.33	1.37
0.430	0.523	21.6	1.56	1.39
0.436	0.523	20.0	1.42	1.11
0.440	0.526	19.5	1.47	1.23
0.215	0.302	40.5	1.03	1.33
0.218	0.305	39.9	1.00	1.26
0.220	0.306	39.1	1.08	1.40
0.241	0.337	39.8	1.17	1.37
0.242	0.339	40.1	1.06	1.22
0.250	0.339	35.6	1.10	1.27
0.301	0.433	43.9	1.25	1.17
0.305	0.435	42.6	1.38	1.31
0.311	0.436	40.2	1.32	1.25
0.311	0.434	39.5	1.27	1.23
0.315	0.436	38.4	1.21	1.11
0.320	0.439	37.2	1.42	1.32
0.430	0.606	40.9	1.67	1.21
0.436	0.610	39.9	1.52	1.34
0.440	0.612	39.1	1.58	1.06
0.215	0.347	61.4	1.03	1.30
0.218	0.349	60.1	1.11	1.24
0.220	0.350	59.1	1.06	1.37
0.241	0.385	59.8	1.18	1.26
0.242	0.388	60.3	1.12	1.34
0.250	0.389	55.6	1.08	1.21
0.301	0.497	65.1	1.41	1.28
0.305	0.498	63.3	1.32	1.22
0.311	0.500	60.8	1.28	1.15
0.311	0.498	60.1	1.42	1.33
0.315	0.501	59.0	1.31	1.09
0.320	0.502	56.9	1.24	1.21
0.430	0.694	61.4	1.67	1.17
0.436	0.695	59.4	1.63	1.28
0.440	0.698	58.6	1.58	1.02

TABLE X(Continued).
Dual-Cylinder Tests Results for Primary Configuration.

Left (Fixed) Velocity Ratio	Rt. (Variant) Velocity Ratio	Left Vertical Force (N)	Right Vertical Force (N)	Left Horizontal Force (N)	Right Horizontal Force (N)
0.215	0.262	1.851	2.238	2.924	2.798
0.218	0.259	1.787	2.210	2.735	2.651
0.220	0.264	2.083	2.251	3.029	3.072
0.241	0.289	1.875	1.942	2.471	2.335
0.242	0.291	1.568	1.908	1.230	2.996
0.250	0.293	1.687	1.926	2.318	2.181
0.301	0.373	1.186	1.288	1.237	1.217
0.305	0.374	1.340	1.402	1.423	1.381
0.311	0.376	1.258	1.299	1.340	1.299
0.311	0.372	0.785	0.838	0.851	0.812
0.315	0.374	0.739	0.792	0.746	0.732
0.320	0.377	0.851	0.904	0.910	0.898
0.430	0.523	0.790	0.851	0.752	0.710
0.436	0.523	0.647	0.847	0.615	0.553
0.440	0.526	0.742	0.804	0.668	0.626
0.215	0.302	1.856	2.478	2.926	2.670
0.218	0.305	1.782	2.426	2.732	2.570
0.220	0.306	2.087	2.457	3.024	2.867
0.241	0.337	1.879	2.109	2.473	2.196
0.242	0.339	1.564	2.049	1.232	2.926
0.250	0.339	1.683	2.066	2.315	2.013
0.301	0.433	1.183	1.394	1.234	1.178
0.305	0.435	1.346	1.499	1.426	1.275
0.311	0.436	1.254	1.468	1.342	1.235
0.311	0.434	0.783	0.893	0.853	0.770
0.315	0.436	0.742	0.855	0.742	0.723
0.320	0.439	0.855	1.019	0.907	0.835
0.430	0.606	0.795	0.962	0.752	0.521
0.436	0.610	0.643	0.956	0.612	0.798
0.440	0.612	0.745	0.917	0.664	0.451
0.215	0.347	1.781	2.553	2.730	2.740
0.218	0.349	2.085	2.585	3.021	2.196
0.220	0.350	1.854	2.606	2.927	2.837
0.241	0.385	1.881	2.141	2.472	1.822
0.242	0.388	1.682	2.135	2.315	2.249
0.250	0.389	1.566	2.115	1.231	2.892
0.301	0.497	1.348	1.559	1.426	1.213
0.305	0.498	1.256	1.466	1.340	1.175
0.311	0.500	1.185	1.454	1.233	1.138
0.311	0.498	0.854	1.020	0.906	0.849
0.315	0.501	0.785	0.944	0.851	0.587
0.320	0.502	0.743	0.893	0.741	0.856
0.430	0.694	0.797	0.960	0.750	0.481
0.436	0.695	0.747	0.968	0.665	0.681
0.440	0.698	0.644	1.018	0.611	0.462

TABLE X (Continued).
Dual-Cylinder Tests Results for Primary Configuration.

Left (Fixed) Cylinder Velocity Ratio	Right (Variant) Cylinder Velocity Ratio	Percent Difference in Velocity Ratios	Lift Coefficient	Drag Coefficient
0.216	0.172	-20.4	0.80	1.33
0.218	0.174	-20.2	0.76	1.42
0.219	0.175	-20.1	0.95	1.45
0.240	0.193	-19.6	0.94	1.27
0.242	0.195	-19.4	1.07	1.39
0.247	0.198	-19.8	0.83	1.47
0.302	0.246	-18.5	1.10	1.22
0.305	0.248	-18.7	1.27	1.41
0.311	0.249	-19.9	1.20	1.33
0.309	0.248	-19.7	1.15	1.32
0.314	0.250	-20.4	1.08	1.39
0.318	0.253	-20.4	1.35	1.16
0.431	0.349	-19.0	1.45	1.42
0.436	0.349	-20.0	1.11	1.19
0.437	0.351	-19.7	1.34	1.29
0.216	0.131	-39.4	0.75	1.45
0.218	0.130	-40.4	0.71	1.34
0.219	0.133	-39.3	0.92	1.47
0.240	0.143	-40.4	1.02	1.42
0.242	0.145	-40.1	0.75	1.28
0.247	0.146	-40.9	0.89	1.49
0.302	0.187	-38.1	1.05	1.24
0.305	0.185	-39.3	1.22	1.45
0.311	0.187	-39.9	1.17	1.35
0.309	0.186	-39.8	1.11	1.34
0.314	0.188	-40.1	1.04	1.18
0.318	0.190	-40.3	1.28	1.41
0.431	0.261	-39.4	1.41	1.41
0.436	0.262	-39.9	1.10	1.22
0.437	0.265	-39.4	1.33	1.30
0.216	0.088	-59.3	0.71	1.50
0.218	0.087	-60.1	0.64	1.48
0.219	0.089	-59.4	0.78	1.36
0.240	0.095	-60.4	0.73	1.29
0.242	0.097	-59.9	0.89	1.45
0.247	0.098	-60.3	0.81	1.52
0.302	0.123	-59.3	0.91	1.37
0.305	0.123	-59.7	0.96	1.26
0.311	0.125	-59.8	1.06	1.47
0.309	0.122	-60.5	0.90	1.21
0.314	0.125	-60.2	1.08	1.42
0.318	0.127	-60.1	0.97	1.37
0.431	0.174	-59.6	1.39	1.31
0.436	0.172	-60.6	1.03	1.24
0.437	0.177	-59.5	1.21	1.39

TABLE X (Continued).
Dual-Cylinder Tests Results for Primary Configuration.

Left (Fixed) Velocity Ratio	Rt. (Variant) Velocity Ratio	Left Vertical Force (N)	Right Vertical Force (N)	Left Horizontal Force (N)	Right Horizontal Force (N)
0.216	0.172	1.852	1.514	2.925	2.671
0.218	0.174	1.789	1.409	2.734	3.241
0.219	0.175	2.082	1.915	3.030	3.071
0.240	0.193	1.689	1.515	2.318	2.010
0.242	0.195	1.878	1.769	2.470	2.267
0.247	0.198	1.564	1.265	1.231	3.779
0.302	0.246	1.186	1.082	1.236	1.279
0.305	0.248	1.341	1.277	1.424	1.483
0.311	0.249	1.256	1.218	1.341	1.401
0.309	0.248	0.784	0.733	0.851	0.891
0.314	0.250	0.741	0.684	0.748	1.086
0.318	0.253	0.929	0.852	0.912	0.619
0.431	0.349	0.791	0.734	0.753	0.741
0.436	0.349	0.649	0.519	0.617	0.635
0.437	0.351	0.741	0.669	0.671	0.686
0.216	0.131	1.855	1.301	2.927	3.174
0.218	0.130	1.783	1.204	2.732	2.906
0.219	0.133	2.086	1.785	3.026	3.159
0.240	0.143	1.877	1.599	2.475	2.365
0.242	0.145	1.562	0.994	1.232	3.130
0.247	0.146	1.681	1.352	2.310	2.764
0.302	0.187	1.182	0.983	1.236	1.321
0.305	0.185	1.345	1.170	1.428	1.562
0.311	0.187	1.252	1.160	1.343	1.440
0.309	0.186	0.782	0.683	0.854	0.914
0.314	0.188	0.740	0.632	0.745	0.812
0.318	0.190	0.852	0.837	0.909	0.952
0.431	0.261	0.793	0.690	0.751	0.732
0.436	0.262	0.641	0.516	0.615	0.668
0.437	0.265	0.745	0.654	0.668	0.700
0.216	0.088	1.853	1.134	2.928	3.383
0.218	0.087	1.781	0.912	2.735	3.492
0.219	0.089	2.082	1.200	2.698	3.024
0.240	0.095	1.563	0.925	1.233	3.164
0.242	0.097	1.880	1.153	2.472	2.470
0.247	0.098	1.679	1.082	2.318	2.862
0.302	0.123	1.185	0.691	1.233	1.592
0.305	0.123	1.255	0.724	1.254	1.344
0.311	0.125	1.346	0.839	1.427	1.604
0.309	0.122	0.742	0.446	0.745	0.855
0.314	0.125	0.851	0.574	0.909	0.965
0.318	0.127	0.782	0.498	0.854	0.954
0.431	0.174	0.792	0.670	0.626	0.752
0.436	0.172	0.641	0.443	0.614	0.690
0.437	0.177	0.744	0.529	0.669	0.793

TABLE XI.
Thirty Degree Offset Tests Results.

Normal Velocity (ft/s)	Left and Right RPM	Left and Right Velocity Ratio	Lift Coefficient	Drag Coefficient
100	5000	0.218	0.93	1.33
100	4950	0.216	0.87	1.42
90	5050	0.246	0.96	1.30
90	5100	0.247	1.04	1.38
70	5000	0.311	1.21	1.28
70	5050	0.314	1.28	1.35
56	4000	0.311	1.15	1.21
56	3900	0.303	1.25	1.30
50	5000	0.436	1.34	1.23
50	5100	0.444	1.46	1.34
50	6000	0.523	1.45	1.15
50	6050	0.527	1.57	1.27

Vita

Captain Walter Clay Howerton was born on 11 July 1966 in Paducah, Kentucky. He attended Paducah Tilghman High School, from which he graduated as valedictorian in May, 1984. On 6 July of that same year he joined the U. S. Air Force, entering the class of 1988 at the Air Force Academy in Colorado Springs. After graduating with a degree of Bachelor of Science in Aeronautical Engineering and receiving his commission as a Second Lieutenant, he was stationed at Edwards Air Force Base, California, for three years. There he worked as a flight test engineer in the 6510th Test Wing on such projects as the MC-130H Combat Talon II and the F-15E Strike Eagle. In June, 1991, he entered the School of Engineering at the Air Force Institute of Technology to pursue a Master's degree in Aeronautical Engineering.

Permanent Address: 3954 Primrose Place
Paducah, Kentucky 42001

REPORT DOCUMENTATION PAGE

Form Approved
OMB No. 0704-0188

Public reporting burden for this collection of information is estimated to average 1 hour per response, including the time for reviewing instructions, searching existing data sources, gathering and maintaining the data needed, and completing and reviewing the collection of information. Send comments regarding this burden estimate or any other aspect of this collection of information, including suggestions for reducing this burden, to Washington Headquarters Services, Directorate for Information Operations and Reports, 1215 Jefferson Davis Highway, Suite 1204, Arlington, VA 22202-4302, and to the Office of Management and Budget, Paperwork Reduction Project (0704-0188), Washington, DC 20503.

1. AGENCY USE ONLY (Leave blank)		2. REPORT DATE December 92	3. REPORT TYPE AND DATES COVERED Master's Thesis	
4. TITLE AND SUBTITLE Experimental Investigation of the Aerodynamics of Independently Rotating Cylindrical Shells			5. FUNDING NUMBERS	
6. AUTHOR(S) Walter Clay Howerton				
7. PERFORMING ORGANIZATION NAME(S) AND ADDRESS(ES) Air Force Institute of Technology Wright-Patterson AFB, Ohio			8. PERFORMING ORGANIZATION REPORT NUMBER AFIT/GAE/ENY/92D-11	
9. SPONSORING / MONITORING AGENCY NAME(S) AND ADDRESS(ES) PL/SXAI Hanscom AFB, MA 01731			10. SPONSORING / MONITORING AGENCY REPORT NUMBER	
11. SUPPLEMENTARY NOTES				
12a. DISTRIBUTION / AVAILABILITY STATEMENT Approved for public release; Distribution Unlimited			12b. DISTRIBUTION CODE	
13. ABSTRACT (Maximum 200 words) The purpose of this thesis was to investigate experimentally the aerodynamic forces on two adjacent, independently rotating cylinders in a cross-flow. This investigation involved a force measurement setup which had the two cylinders mounted on a common support shaft, extending beyond the span of the wind tunnel test section, and supported by spoke rings with strain gages in the vertical and horizontal directions. This setup proved capable of measuring aerodynamic forces. The lift on the independently rotating cylinders was found to increase as one cylinder's angular speed increased while the other's remained constant, and decrease as the relative angular rate decreased. The drag coefficient was fairly constant over the range of velocity ratios tested, and minimal changes were noted with relative changes in angular speeds. Interactions between the two cylinders had the most effect on the lift and drag above 40% disparity in the angular rotation rates. The investigation also showed that for an offset angle of 30° on an approximately two-dimensional cylinder, the normal component of freestream velocity may be treated as the only significant contributor to the forces on the cylinder.				
14. SUBJECT TERMS Rotating Cylinders, Lift, Drag, Velocity Ratio			15. NUMBER OF PAGES 90	
			16. PRICE CODE	
17. SECURITY CLASSIFICATION OF REPORT Unclassified	18. SECURITY CLASSIFICATION OF THIS PAGE Unclassified	19. SECURITY CLASSIFICATION OF ABSTRACT Unclassified	20. LIMITATION OF ABSTRACT UL	